ASL-TR-0003

LEVEL II

MIE THEORY SENSITIVITY STUDIES - THE EFFECTS OF AEROSOL COMPLEX REFRACTIVE INDEX AND SIZE DISTRIBUTION VARIATIONS ON EXTINCTION AND ABSORPTION COEFFICIENTS PART II: ANALYSIS OF THE COMPUTATIONAL RESULTS

MARCH 1978

By

S.G. Jennings

J.B. Gillespie

US Army Electronics Research and Development Command

Atmospheric Sciences Laboratory

White Sands Missile Range, N.M. 88002

NOTICES

Disclaimers

The findings in this report are not to be construed as an official Department of the Army position, unless so designated by other authorized documents.

The citation of trade names and names of manufacturers in this report is not to be construed as official Government indorsement or approval of commercial products or services referenced herein.

Disposition

Destroy this report when it is no longer needed. Do not return it to the originator.

SECURITY CLASSIFICATION OF THIS PAGE (When Data Entered)

REPORT DOCUMENTATION PAGE

READ INSTRUCTIONS BEFORE COMPLETING FORM

1. REPORT NUMBER: ASL-TR-0003

2. GOVT ACCESSION NO.

3. RECIPIENT'S CATALOG NUMBER

4. TITLE (and Subtitle): MIE THEORY SENSITIVITY STUDIES, & THE EFFECTS OF AEROSOL COMPLEX REFRACTIVE INDEX AND SIZE DISTRIBUTION VARIATIONS ON EXTINCTION AND ABSORPTION COEFFICIENTS. PART II: ANALYSIS OF THE COMPUTATIONAL RESULTS

5. TYPE OF REPORT & PERIOD COVERED: R&D Technical Report

6. PERFORMING ORG. REPORT NUMBER

7. AUTHOR(s): S. G. Jennings, J. B. Gillespie

8. CONTRACT OR GRANT NUMBER(s)

Research and Development Technical Rept's

9. PERFORMING ORGANIZATION NAME AND ADDRESS: Atmospheric Sciences Laboratory, White Sands Missile Range, NM 88002

10. PROGRAM ELEMENT, PROJECT, TASK AREA & WORK UNIT NUMBERS: DA Task No. 1L/161102B53A

11. CONTROLLING OFFICE NAME AND ADDRESS: US Army Electronics Research and Development Command, Adelphi, MD 20783

12. REPORT DATE: Mar[illegible]78

13. NUMBER OF PAGES: 88

14. MONITORING AGENCY NAME & ADDRESS (if different from Controlling Office): 1L161102B53A

15. SECURITY CLASS. (of this report): UNCLASSIFIED

15a. DECLASSIFICATION/DOWNGRADING SCHEDULE

16. DISTRIBUTION STATEMENT (of this Report): Approved for public release; distribution unlimited. 88 p.

17. DISTRIBUTION STATEMENT (of the abstract entered in Block 20, if different from Report)

18. SUPPLEMENTARY NOTES: ERADCOM/ASL-TR-0003

19. KEY WORDS (Continue on reverse side if necessary and identify by block number)

Complex refractive index
Extinction coefficient
Absorption coefficient
Particle size distribution
Real index of refraction
Imaginary index of refraction
Middle IR propagation

20. ABSTRACT (Continue on reverse side if necessary and identify by block number)

A comprehensive study has been made of the effect of the complex index of refraction and particle size distribution on the volume extinction and absorption coefficients. Calculations were performed by use of a generalized Mie scattering program for lognormal particle size distributions over a range of geometric mean radius r_g from 0.005 μm to 10 μm and geometric standard deviation σ_g from 1.0 up to 2.5. The results are normalized to a total particle mass loading of 100 g/m^{-3} and a particle density of 2.5 g/cm^{-3}. The computations were made at

DD FORM 1 JAN 73 1473 EDITION OF 1 NOV 65 IS OBSOLETE

SECURITY CLASSIFICATION OF THIS PAGE (When Data Entered)

20. ABSTRACT (cont)

wavelength λ of 0·55, 0·6943, 1·06, 3·8 and 10·6 micrometers, for a range of imaginary index k from 0·001 to 6·0 and a range of real index n from 0·1 up to 6·5.

The extinction σ_E is insensitive to imaginary index k for $0{\cdot}001 \lesssim k \lesssim 0{\cdot}025$ providing $0{\cdot}01 < r_g/\lambda \leq 0{\cdot}2$, $\sigma_g \gtrsim 2.0$ and $\lambda \leq 1{\cdot}06\mu m$, while the ratio of the extinction at real index 1·8 compared to the value at n = 1·33 varies by up to a factor of about 4·0 for identical parameters. Extinction becomes nearly independent of both real index n and imaginary index k for $r_g/\lambda \lesssim 0{\cdot}2$, $\sigma_g \gtrsim 1{\cdot}5$, which represents most measured atmospheric size distributions for $0{\cdot}001 \leq k \leq 2{\cdot}0$ and $1{\cdot}4 \leq n \leq 2{\cdot}5$ providing $0{\cdot}55\mu m\ \lambda \leq 1{\cdot}06\mu m$. The absorption σ_A is insensitive to n for $0{\cdot}01 \leq r_g/\lambda \leq 10$, while σ_A varies linearly with k providing $0{\cdot}001 \lesssim k \lesssim 0{\cdot}01$, $r_g/\lambda \leq 0{\cdot}5$ and $\sigma_g \leq 2{\cdot}0$.

Absorption is independent (within a factor of approximately 3) of r_g for r_g/λ 0·75 with $k \leq 0{\cdot}05$ which represents a reasonably wide range of realistic atmospheric values. The extinction σ_E decreases as $1/r_g$ for $r_g/\lambda \gtrsim 0.5$ and $\gtrsim 0.25$ for the spectral ranges $0.55\mu m \leq \lambda \leq 1.06\mu m$ and $3.8\mu m \leq \lambda \leq 10.6\mu m$, respectively, for $k \lesssim 0.5$.

The real index n significantly affects σ_E and σ_A for $3{\cdot}8\mu m \leq \lambda \leq 10{\cdot}6\mu m$ and extinction is mainly dependent on n over a wide range of r_g and σ_g. The extinction σ_E is well approximated by $\sigma_E = \sigma_{max} \exp \left\{ -\frac{1}{2} \left[\frac{\ln (n/ng)}{\ln \sigma_n} \right]^2 \right\}$ where

σ_{max} is the extinction at $n = n_g$, and σ_n is the geometric deviation of σ_E with reference to n.

Extinction is invariant to k for $0{\cdot}001 \lesssim k \lesssim 8{\cdot}0$ for broad realistic atmospheric distributions in the wavelength range 3·8μm to 10·6μm. Extinction is more sensitive to changes in real index than to imaginary index (up to a factor of about 3) for the majority of atmospheric particle size distributions in the same wavelength range.

The particle size distribution is of major importance in affecting σ_E and σ_A and has greatest influence for $k \leq 0{\cdot}1$. Extinction is constant for $r_g/\lambda \lesssim 0{\cdot}15$ for k = 0·5, for $3{\cdot}8\mu m \leq \lambda \leq 10{\cdot}6\mu m$. The distribution spread σ_g does not appreciably influence the extinction or absorption for realistic values of $r_g \geq 0{\cdot}25\mu m$ and $0{\cdot}005\mu m$, respectively.

CONTENTS

PREFACE

This study was undertaken to answer Army problems associated with electromagnetic propagation and electro-optic sensor systems. The results of this study apply directly to the atmospheric aerosol measurements program and to research associated with the determination of the optical constants of atmospheric particulate matter. The study supplies answers to such questions as which optical quantities should be measured and how accurately they should be determined for several important wavelengths. It also gives insight to the applicability of experimental techniques used to determine the imaginary refractive index of particulates.

The Mie Scattering Computer Code, developed by Gerry W. Grams, N.C.A.R., Boulder, was made available by R. G. Pinnick. Much appreciated help was given by Don Hoihjelle and Gilbert Fernandez in the initial stages of the computer programming work. Gratitude is accorded to Ken Webb for diligent work in reducing the computer data to graphical form. Thanks are extended to J. Lentz and K. O. White for constructive suggestions.

MIE THEORY SENSITIVITY STUDIES

THE EFFECTS OF AEROSOL COMPLEX REFRACTIVE INDEX AND SIZE DISTRIBUTION VARIATIONS ON EXTINCTION AND ABSORPTION COEFFICIENTS

PART II: ANALYSIS OF THE COMPUTATIONAL RESULTS

INTRODUCTION

The importance of the effects of atmospheric aerosols on the operation of electro-optical devices has increased considerably during recent years. In addition, aerosols affect radiative transfer balance in the atmosphere and hence climate. An important contribution to the heat budget of the atmosphere is attributed to absorbed radiation by polydispersions of aerosols.

The usual procedure for estimating these effects is to assume that the aerosol is composed of homogeneous spherical particles and use Mie theory [1] to calculate the scattering parameters for radiation attenuation, discernibility of targets, etc. The input parameters required for Mie calculations are (1) particle size distribution, (2) particle number density, and (3) particle refractive index as a function of radiation wavelength. Since aerosol size distribution and refractive index are in practice difficult quantities to measure, a theoretical study to assess the relative importance of these quantities in radiation calculations is imperative. In this report the authors investigate the effects of particle size distribution and real and imaginary parts of the refractive index on volume extinction and absorption coefficients for families of size distributions and ranges of refractive index that are reasonable for aerosols in the atmosphere. This theoretical sensitivity study has been performed

for selected wavelengths from the visible (0.55μm) to the middle-infrared (10.6μm). Effects of polydispersions of aerosol containing particles of mixed composition and irregular particles have not been addressed.

COMPUTATIONAL DETAILS

A generalized Mie code developed by G. W. Grams of the National Centre for Atmospheric Research was used. The Mie theoretical formalisms have already been described by several workers [2-4] and will not be further discussed here. The program was verified with a MIE-2 program of Blättner [5] and with that of Grams [6] using a different computer. The results of the calculations are presented in the form of volume extinction coefficient σ_E (km^{-1}), volume scattering coefficient σ_S (km^{-1}) and volume absorption coefficient σ_A (km^{-1}) where, for example, σ_E is given by

$$\sigma_E = \int_{\tau_1}^{\tau_2} \pi r^2 Q_{ext}(x,m)\, n(r)dr, \qquad (1)$$

where n (r) is the particle differential size distribution, Q_{ext} is the efficiency factor for extinction and is a function of the particle complex index of refraction m and the size parameter $2\pi r/\lambda$. Here, the complex index of refraction $m = n - ik$, where n is the real part of the refractive index and k the imaginary (absorptive) part. The particle radius and radiation wavelength are denoted by r and λ, respectively. All computations are performed with the number of particles per logarithmic radius internal, dn/d ln r given by

$$\frac{dN}{d \ln r} = \frac{1}{\sqrt{2\pi} \ln \sigma_g} \exp\left\{-\frac{1}{2}\left[\frac{\ln(r/r_g)}{\ln \sigma_g}\right]^2\right\} \qquad (2)$$

r_g and σ_g are defined as the geometric mean radius and geometric standard deviation, where N is the total number of particles per unit volume.

A lognormal distribution was chosen to represent the particle size distribution for several reasons:

1. It represents desert-type aerosols adequately [7].

2. It also represents urban-particle size measurements [8].

3. Davies [9] has shown that particle size distributions can be well represented by combinations of lognormally distributed values of particle size.

Calculations have been made over a wide range of geometric mean radii, r_g, from 0·005μm up to 10·0μm and geometric standard deviation, σ_g, from 1·0 up to 2·5. The results have been normalized arbitrarily to a total particle mass of 100μg m^{-3} with a uniform particle density of 2·5 g cm^{-3}, consistent with measurements of maritime and dry urban aerosols by Hanel [10].

APPROXIMATION FOR THE REGIMES $r/\lambda \ll 1$; $|mx| < 1$, $r/\lambda \gg 1$

Regime $r/\lambda \ll 1$, $|mx| < 1$

This is the regime for particles small compared to the wavelength and for small phase shifts. A small phase shift implies that the phase difference between the incident and scattered radiation fields is small. van de Hulst [2] has shown that the efficiency factor of absorption, Q_A, can be expressed as the series expansion

$$Q_A = - \text{Imag} \left[4x\left(\frac{m^2 - 1}{m^2 + 2}\right) + \frac{4}{15} x^3 \left(\frac{m^2 - 1}{m^2 + 2}\right)^2 \cdot \frac{m^4 + 27\, m^2 + 38}{2m^2 + 3} \right], \quad (3)$$

and Q_S, the efficiency factor for scattering can be written as

$$Q_S = x^4 \cdot 8/3 \, \text{Re}\left(\frac{m^2 - 1}{m^2 + 2}\right)^2, \quad (4)$$

where $x = 2\pi r/\lambda$ and $m = n - ik$.

For the small particle and phase shift limit, ($r << \lambda$), $|mx| < 1$, Eq. (3) becomes

$$Q_{ext} = -4 \quad \chi \, \mathrm{Im} \left(\frac{m^2 - 1}{m^2 + 2} \right). \tag{5}$$

This can be written as

$$Q_A = \frac{2\pi r}{\lambda} \cdot \frac{24\ nk}{(n^2 - k^2 + 2)^2 + (2nk)^2} \cdot \tag{6}$$

The absorption coefficient, σ_a, for a particle of radius r can be written as

$$\sigma_a = \pi r^2 \, Q_A. \tag{7}$$

Therefore, the absorption per unit mass in Eq. (7) can be written as

$$\frac{\sigma_a}{m} = \sigma_A = \frac{\pi r^2}{4\pi/3 \ r^3 \rho} \cdot Q_A = \frac{3}{4\rho r} \ Q_A, \tag{8}$$

where ρ is the particle density.

Therefore, the absorption coefficient per unit mass, σ_A, for small particles and small phase shifts can be written as

$$\sigma_A = \frac{3}{4\rho} \frac{2\pi}{\lambda} \cdot \frac{24\ nk}{(n^2 - k^2 + 2)^2 + (2nk)^2} \cdot \tag{9}$$

Various relationships between σ_A and the optical constants n and k are now established below for $r/\lambda << 1$, $|mx| << 1$. The absorption, σ_A, can be represented by the expression

$$\sigma_A = \text{constant} \cdot \frac{nk}{(n^2 - k^2 + 2)^2 + (2nk)^2}, \tag{10}$$

where it is assumed that n and k are invariant with wavelength λ.

1. $n = k$: Then σ_A becomes $\sigma_A = \frac{k^2}{4 + 4k^4} = \frac{n^2}{4 + 4n^4}$ (11)

2. $n > k$. $\sigma_A = \text{constant} \quad \frac{nk}{(n^2 + 2)^2}$, (12)

or proportional to k for a fixed value of n, and proportional to

$$\frac{n}{(n^2 + 2)^2} \tag{13}$$

for a fixed value of k.

3. $k > n$. $\sigma_A = \text{constant} \cdot \frac{nk}{(2 - k^2)^2}$ (14)

Therefore, σ_A is proportional to n for constant k and σ_A is proportional to

$$\frac{k}{k^4 - 2k^2 + 4} \tag{15}$$

for a fixed value of n.

Geometrical Optics Approximation, $r >> \lambda$

It is known by physical argument, for example the work of van de Hulst [2] and Chylek [11], that the limit of the extinction efficiency is 2 for $r >> \lambda$. Therefore the volume extinction coefficient for a distribution n (r) is twice the geometrical cross-sectional area of the polydispersion of particles, with the assumption that all of the particles in the distribution satisfy the $r/\lambda >> 1$ condition. This approximation is discussed further in the appendix.

COMPLEX REFRACTIVE INDEX FOR SEVERAL ATMOSPHERIC AEROSOL CONSTITUENTS

Atmospheric aerosols normally contain a number of constituents; the dominant one (from the point of view of radiation transfer) generally varies with location. Because of the nonlinearity of Mie theory, no single set of optical constants can adequately characterize the aerosol.

For this reason, more information is required of the constituents of natural aerosols. Mixtures of particle types are probably prevalent, which renders the determination of the refractive index of the mixture difficult and probably ambiguous. Nevertheless, knowledge of a reasonably wide range of the more commonly found atmospheric constituents is available. Table 1 gives a range of minimum and maximum values of both the real and imaginary part of the complex index of refraction for ammonium sulfate, sodium chloride, water, quartz (crystalline form), sulfuric acid solutions, ammonium sulfate solutions, carbon, and atmospheric dust over relatively narrow wavelength ranges. Toon and Pollack [12] have given a comprehensive set of values of ammonium sulfate (crystalline form), and Table 1 shows their extreme values for the three wavelength bands 0·5μm to 1·0μm, 3·0μm to 5·0μm, and 9·0μm to 11·0μm. Values of the indices for ammonium sulfate solutions have been taken from the work of Downing et al. [13]. Their extrapolation of the number densities of the ions present in crystalline ammonium sulfate gives good agreement with the values of Toon et al. [12].

Toon et al. [12] have presented the refractive indices for crystalline NaCl. Table 1 shows the extreme values for the three wavelength ranges. Querry et al. [14] have recently published refractive index values of aqueous solutions of NaCl (0·25 M and 0·5 M) which closely correspond to values of solutions found in the oceans.

The index values of bulk crystalline quartz (a constituent of desert aerosols) are taken from Spitzer and Kleinman [16] and possess extreme values of n and k from 0·1 up to 7·5 and from 0·015 up to 7·5

in the wavelength region from 9μm to 11μm. Since crystalline quartz is birefringent, calculations for the ordinary and extraordinary rays are weighted 2 to 1 following the procedure of Peterson and Weinman [17].

Palmer and Williams [18] give the optical constants of sulfuric acid solutions (which are found in the stratosphere and troposphere) for solution concentrations of 25, 38, 50, 75, 84.5, and 95 percent. Table 1 shows the values for solution concentrations of 25, 50, and 75 percent for the three wavelength ranges.

Carbon is a common constituent in the atmosphere which constitutes about 0·5 to 1·5 percent of the aerosol in desert-type aerosols and may approach up to 10 to 15 percent of the aerosol mass in urban industrial areas. A range of values for the refractive index values for carbon [19, 20] taken from the summarized values of Twitty and Weinman [21] are shown in the table.

The optical constants of montmorillonite have been determined by Toon et al. [25] who used both Kramers-Kronig and dispersion techniques over a wavelength range from 5μm to 40μm. Their extreme values are shown in Table 1. There is a relatively wide variation in the values of the optical constants in the 9μm to 11μm range.

The complex index of refraction of atmospheric dust can be determined by a number of methods, and Fischer [26, 27], Lindberg and Laude [28], Hanel [10], Herman et al. [29], Grams et al. [30], Patterson et al. [31], and others have reported measurements. Some selected values are given in Table 2.

Few values of imaginary index of refraction exist for the wavelength ranges 3μm to 5μm and 9μm to 11μm. Fischer [27] has derived values of the mass absorption index k/ρ in these ranges, but values of the aerosol particle density must be assumed.

Few measurements are available for the real index of refraction for atmospheric dust in the middle infrared regime. Soil-derived aerosols are composed of a majority of clay minerals as shown by Hoidale and Blanco [32]. The refractive indices of these clay minerals in the 3μm to 5μm and 9μm to 11μm range are unknown.

A summary from Tables 1 and 2 of the range of complex refractive index values over these wavelength ranges of 0·55μm to 1·06μm, 3·0μm to 5·0μm, and 9·0μm to 11·0μm is shown in Table 3. The extreme values for the 9·0μm to 11·0μm wavelength range are due to quartz, while the upper values in the two remaining wavelength bands are due to carbon.

PARTICLE SIZE DISTRIBUTION PARAMETERS FOR MEASURED POLYDISPERSIONS OF AEROSOLS

Lognormal parameters for measured distributions of urban, maritime, continental, desert aerosols, and fog are shown in Table 4. Most of the distributions possess values of geometric mean radius and standard geometric deviation between about 0·1μm to 5·0μm and from about 1·5μm to 2·5μm, respectively. For lognormal components with $r_g << 0{\cdot}1\mu m$, the contribution of the distributions to extinction can usually be regarded as negligible because of their minimal mass loading. The role of submicrometer particles on the scattering parameters will be discussed later in the report.

COMPUTATIONAL RESULTS

The computational results are presented in tabulated form by Jennings [32]. These tabulated results of volume extinction coefficient σ_E, are now analyzed in the form of graphical plots and tables. For the sake of brevity, only a relatively small cross-section of the results is presented. However, the results in this cross section are representative. The results are divided into two main categories:

Wavelength range 0·55μm to 1·06μm

Wavelength range 3·8μm to 10·6μm

Wavelength Range 0·55μm to 1·06μm

Volume Extinction Coefficient and Volume Absorption Coefficient as a Function of Real Index of Refraction. Values of volume extinction and volume absorption coefficients for a particle mass loading of 100μg m^{-3} are shown in Figures 1 and 2 for λ = 0·55μm, and in Figure 3 for λ = 1·06μm. The real index of refraction n ranges from 1·0 to 2·5 for the imaginary index k = 0·01. Table 5 gives the range of geometric mean radius r_g and geometric standard deviation σ_g used in the above figures.

The following conclusions are drawn from the results:

1. The ratio of $\sigma_E(n = 1{\cdot}8)/\sigma_E(n = 1{\cdot}33)$ for $r_g/\lambda \leq 0{\cdot}02$ and $\sigma_g \leq 1{\cdot}5$ is reduced to about 0·75 as shown in Table 6. The maximum value of σ_E (n = 1·8)/σ_E (n = 1·33) is about 5·0 for the larger r_g/λ values. Also shown are values of the ratio σ_E $(n_1)/\sigma_E$ (n_2), where n_1, n_2 decrease with increasing values of imaginary index k for the same size distribution.

2. The extinction coefficient, σ_E, becomes almost independent of the real index n over the range $1.3 \leq n \leq 2.5$ for values of $r_g/\lambda \geq 0.5$

(see Figures 2 and 3). The dependence of σ_E on n becomes less for increasing values of σ_g because the large sphere approximation ($r >> \lambda$) now prevails where σ_E becomes independent of the optical constants n and k and solely dependent on the integrated cross-sectional area of the particles in the distribution.

3. Equations (3) and (4) show that the extinction is equal to the absorption for the condition $r/\lambda \lesssim 0.1$, and for $|mx| < 1$. However, this is no longer true as the spread (σ_g) of the distribution increases as is evident from Figures 1 and 2 for $\sigma_g = 2.5$ and Figures 1 and 3 for values of $\sigma_g = 1.5$, 2.0, and 2.5.

4. The volume absorption coefficient is relatively insensitive to variations in the real index, n, and independent of σ_g over the r_g range from 0.005 up to 5.0μm as illustrated in Figures 1 to 3. According to Eq. (13), the absorption σ_A decreases slowly with increasing n, i.e., $n/(n^2 + 2)^2$ for $n >> k$ in the small particle regime, for uniform sized particles. An increase in σ_g causes the absorption to increase slowly with increasing n (Figures 1 and 3). The absorption becomes independent of n for $r_g/\lambda \gtrsim 2.0$.

Volume Extinction Coefficient and Volume Absorption Coefficient as a Function of Imaginary Index of Refraction for $0.55\mu m \leq \lambda \leq 1.06\mu m$. The extinction is nearly equal to the absorption for steeper size distributions for which $r_g/\lambda \leq 0.1$ (Figures 4 and 6) for constant values of n. However, the extinction becomes constant with imaginary index k for increasing values of r_g and σ_g (Figures 4, 5, and 6). This finding is summarized in Table 7 where the range of imaginary index k over which

the extinction is nearly constant is tabulated for a wide range of r_g/λ and σ_g values. The extinction is insensitive to k for $r_g/\lambda \gtrsim 0{\cdot}2$. This result corroborates the findings of Patterson et al. [38] that a variation in k from 0 to 0.05 had negligible effect on the comparison between measured and calculated visibilities for $\sigma_g \simeq 2.0$ and $r_g \simeq 0.5\mu m$.

The absorption coefficient varies linearly with k for geometric mean radii $r_g \lesssim 0.1\mu m$, irrespective of σ_g for $\sigma_g \leq 2.5$. This is in agreement with the small particle approximation [Eq. (12)]. More generally, maximum values of k for which linearity of σ_A with k (within ± 20 percent) ceases for $\lambda = 0.55\mu m$ and $1.06\mu m$, are shown in Tables 8 and 9 for appropriate r_g and σ_g values. The linearity of σ_A with k ceases for increasing r_g/λ and σ_g values.

The dependence of absorption on k (Figures 4, 5, and 6) is characterized by a steady increase in absorption with increasing k, then a plateau where absorption is constant, followed by a decrease in absorption for increasing values of k. The absorption becomes constant for $k > k_c$, and values of k_c are tabulated in Tables 10 and 11 for realistic values of r_g and σ_g for $\lambda = 0{\cdot}55\mu m$ and $1{\cdot}06\mu m$. The absorption becomes insensitive for k values between 0·025 and 0·05 for most particle size distributions in this wavelength regime.

The Dependence of Extinction Coefficient and Absorption Coefficient on Particle Size for $0.55\mu m < \lambda < 1.06\mu m$. Bergstrom [39] discussed the extinction and absorption coefficients of the atmospheric aerosol as a function of particle size for uniform particles and for a narrow range

of power low and lognormal distributions. He used a relatively narrow range of optical constants.

Plots of σ_E and σ_A as a function of r_g and σ_g are presented in Figures 7 and 8, for real indices of 1.6, 1.7, and a number of imaginary index values for wavelengths 0.55μm and 1.06μm.

The absorption per unit mass is nearly independent of geometric mean radius (within a factor of 3) for $r_g/\lambda \leq 0.75$ and $k \leq 0.05$ in agreement with Waggoner et al. [35]. The implications of a constant response of absorption to particle size for certain conditions will be discussed in a subsequent report [36]. For $r/\lambda \ll 1$, Eq. (9) predicts a constant value of absorption coefficient for fixed values of n, k, and λ.

The absorption per unit mass, σ_A, decreases as $1/r_g$ for $r_g/\lambda \gtrsim 7$ for k = 0·01 and $r_g/\lambda \gtrsim 0{\cdot}2$ with k = 0·5. This can be seen from the following considerations: The volume absorption coefficient σ_{ABS} can be written for a polydispersion of particles as:

$$\sigma_{ABS} = \int_{r_1}^{r_2} \pi r^2 \, Q_{ABS} \, n(r) \, dr, \tag{16}$$

where Q_{ABS} is the efficiency factor for absorption. This can be re-written as

$$\sigma_{ABS} = \sqrt{\frac{\pi}{2}} \cdot \frac{N}{\ell n \, \sigma_g} \int_{r_1}^{r_2} Q_{ABS} \, r \exp \left\{ -\frac{1}{2} \left[\frac{\ell n (r/r_g)}{\ell n \, \sigma_g} \right]^2 \right\} dr \tag{17}$$

since

$$n(r) = \frac{N}{\sqrt{2\pi}\ \ell n\ \sigma_g} \quad \frac{1}{r} \quad \exp\left\{-\frac{1}{2}\left[\frac{\ell n(r/r_g)}{\ell n\ \sigma_g}\right]^2\right\} \tag{18}$$

for a lognormal distribution.

Plass [42] has shown that Q_{ABS} becomes constant for $r/\lambda > 1$ for $k > 0.1$, and probably for $k > 0.05$. Therefore, the expression for σ_A reduces to the form

$$\sigma_{ABS} = \text{constant} \int_{r_1}^{r_2} r \exp\left\{-\frac{1}{2}\left[\frac{\ell n(r/r_g)}{\ell n\ \sigma_g}\right]^2\right\} dr \tag{19}$$

The above integral has an identical form to the expression for the total cross-sectional area of a lognormal distribution. Information in the appendix shows that the cross-sectional area per unit volume for a lognormal distribution is proportional to $1/r_g$ for constant σ_g. Therefore, the absorption per unit mass, σ_g, is proportional to $1/r_g$ under the above conditions. The $1/r_g$ relation is valid at increasing values of r_g/λ as k is reduced below 0.05, as is evident from Figures 7 and 8. This corroborates the finding [37] that the efficiency factor for absorption is constant for decreasing k and increasing r/λ.

The extinction coefficient per unit mass, σ_E, is sensitive to r_g, σ_g, and k as shown in Figures 7 and 8. The extinction σ_E rises steeply with r_g, for a given σ_g, peaks and falls as $1/r_g$ for $r_g/\lambda \gtrsim 1.0$. The $1/r_g$ falloff for $r_g/\lambda >> 1$ has been shown in the appendix.

The extinction increases with increasing σ_g, for $r_g/\lambda \lesssim 0.5$, while the extinction decreases with increasing σ_g for $r_g/\lambda \gtrsim 0.5$ and for $k \leq 0.1$. Furthermore σ_E is independent of r_g and σ_g within a factor of about 2 for $r_g/\lambda < 0.25$ (Figures 7 and 8) for $k = 0.5$.

Wavelength Range 3.8 to 10.6 Micrometers

Volume Extinction Coefficient as a Function of Real Index of Refraction n at λ = 3.8μm. The real index of refraction has a significant effect on the volume extinction coefficient σ_E and volume absorption coefficient σ_A for radiation wavelengths 3.8μm $\lesssim \lambda \lesssim$ 10.6μm. The dependence of σ_E and σ_A on n for a wide range of values of r_g and σ_g for constant k is shown in Figures 9 and 10.

The shape of the curves relating σ_E to n can in many cases be approximated to a functional form

$$\sigma_E = \sigma_{Emax} \exp \left\{ -\frac{1}{2} \left[\frac{\ell n(n/n_g)}{\ell n\ \sigma_n} \right]^2 \right\} \qquad (20)$$

where σ_{max} represents the real value of extinction at $n = n_g$ and n is the geometric standard deviation of the n values centered around n_g.

Fitted points satisfying Eq. (20) are shown on σ_E versus n plots in Figure 10 for λ = 3.8μm. Values of the parameters n_g, σ_n which give a good fit to the curves of σ_E versus n over most of the real index range are shown in Table 12.

The relation between extinction and real index of refraction demonstrates clearly from Figures 9 and 10 that: (a) real index n plays a significant role in effecting extinction for a particular size distribution and (b) the particle size distribution is also of major importance in determining the shape of the functional dependence of extinction on real refractive index. The extinction increases with increasing n with the exception of the regime r_g/λ < about 0·015 when the extinction de-

creases according to Eq. (13).

Table 13 gives the range of imaginary index k for which the volume extinction coefficient σ_E is constant within about 15 percent, for $\lambda = 3{\cdot}8\mu m$. It is noteworthy that for constant n (equal to 1·7 here), σ_E is relatively unchanged by variation in k for $r_g \geq 0{\cdot}25$ and $\sigma_g \geq 1{\cdot}5$. The extinction also remains invariant to values of k provided $k \lesssim 0.05$ for the radius range $0.05 \leq r_g \leq 0.25$, for relatively broad ($\sigma \geq 2.0$) distributions. These results lead to the following conclusions:

1. The extinction per unit mass is predominantly dependent on the real index n for values of k given in Table 13. This dependence of σ_E on n can be approximated closely by Eq. (20).

2. In the regime of k where σ_E is linearly proportional to k (values given in Table 11), σ_E can be written as:

$$\sigma_E = c_2 k \exp\left\{-\frac{1}{2}\left[\frac{\ln (n/n_g)}{\ln \sigma_n}\right]^2\right\}, \qquad (21)$$

where $c_2 k$ is equal to σ_{Emax}. Hence c_2 is easily calculable for a specific k.

The increase in extinction at real index = n, compared to n = 1·4 (real index of water at 3·8μm = 1·364) is shown in Table 14 as a function of r_g and σ_g for k = 0·025. The maximum variation of $\sigma_E(n)/\sigma_E(n = 1{\cdot}4)$ is about 2 for $r_g \leq 0.05$ and $\sigma_g \leq 2{\cdot}0$, but possesses values up to 7 for $r_g \geq 0{\cdot}1$ with $\sigma_g \geq 1{\cdot}5$.

The range of k for which σ_E is nearly linear with k at a selection of r_g and σ_g values is given in Table 15. The linearity of σ_E with k only

prevails for the smaller particle range ($\tilde{<}$ 0·1μm).

Comment on the volume absorption coefficient as a function of k, although plotted in Figure 11 for the sake of completeness, will be deferred to a subsequent report [41].

Volume Extinction Coefficient as a Function of Real Index of Refraction at λ = 10.6μm. Figures 12 to 14 show the effect of real index of refraction n on extinction, σ_E, for a wide range of particle size distribution parameters r_g and σ_g. The range of particle distribution parameters used in the above figures is shown in Table 16. The variation of extinction with n can be represented, for most combinations of r_g and σ_g, by an equation similar to Eq. (21), i.e.,

$$\sigma_E = a_1 \exp [-b_1 \ell n^2 (n/ng)] \qquad (22)$$

where a_1 is the maximum extinction value for a given extinction versus real index curve and b_1 is equal to 1/2 · $\ell n\ \sigma_n^2$ where σ_n is a measure of the spread of the σ_E values about the geometric mean n_g.

A set of points satisfying Eq. (22) is plotted along with rigorous Mie results in Figures 15 and 16 for various values of r_g and σ_g.

The parameters of Eq. (22) which give a reasonably good fit to the Mie results over most of the real refractive index range are given in Table 17.

Table 18 presents a summary of computations made of extinction for real refractive index n, ranging between 1·2 and 3·5 compared to values

at n = 1·2 (real index of water at 10·6μm = 1·185), over a wide range of r_g values. The ratio is sensitive to σ_g for any given r_g except for $r_g \leq 0{\cdot}01$. Table 18 represents most combinations of typical parameters of particle size distributions for atmospheric aerosols. The ratio of σ_E (n = 2·5)/σ_E (n = 1·2) attains a maximum value of 11·6 and decreases to a value of about 2·0 at r_g = 2·5μm, σ_g = 2·0. In general, for $r_g \tilde{\leq} 0{\cdot}75\mu m$ the extinction ratio increases with σ_g up to $\sigma_g \leq 2.0$ and thereafter decreases with increasing σ_g.

Volume Extinction Coefficient as a Function of Imaginary Index of Refraction at λ = 10·6μm. The variation of σ_E with k, for n = 1·8 is shown in Figure 17 for λ = 10.6μm. The range of imaginary index k for which σ_E is nearly constant (to within ±15 percent) is summarized in Table 19. The extinction is nearly independent (within ±15 percent) of k, $0{\cdot}001 \leq k \leq 0{\cdot}1$ for broad distributions with r_g = 0·25μm, 0·5μm. Extinction is insensitive (to within ±15 percent) to a wide variation in k ($0{\cdot}001 \leq k \tilde{\leq} 8{\cdot}0$) for $r_g \geq 0{\cdot}75\mu m$ and $\sigma_g \geq 2{\cdot}0$. Since most atmospheric constituents have imaginary index k values within the above range, it is concluded that at 10.6μm wavelength, extinction is relatively independent of k for the broader particle size distributions with geometric mean radii $\tilde{>}$ 0·5μm. Over the range of k for which σ_E is relatively constant, σ_E can be written solely in terms of real index n according to Eq. (20).

Table 20 shows the range of k for which σ_E is linear to within 15 percent, with k, at λ = 10·6μm. The extinction is written in terms of Eq. (21), analogous to the λ = 3·8μm case, for the relevant values of r_g

and σ_g shown in Table 16. Thus, the linearity of σ_E with k exists for particle sizes less than about 0·25μm for values of k typical of atmospheric particulates (from about 0·01 to about 0·5 at λ = 10·6μm). The effect of imaginary index on absorption at λ = 10·6μm will be discussed in a subsequent report [41] which will include a comment on the use of the pellet spectrophone technique [43] as a possible method to determine the imaginary index of atmospheric particulates.

Table 21 summarizes the relative sensitivity of volume extinction coefficient σ_E to changes in imaginary and real index of refraction. The variation in extinction as real index is increased two-fold is compared to the variation in extinction with imaginary index. It is evident that σ_E is more sensitive to changes in n compared to changes in k for the majority of r_g and σ_g values, particularly for values of $r_g \gtrsim$ 0·25μm, where extinction becomes insensitive to k. Most components of measured atmospheric particle size distributions have r_g and σ_g values ranging from about 0·1 to approximately 10μm and from a minimum of about 1·25 to about 2·5, respectively, as seen from Table 4. Since typical values of imaginary index of atmospheric constituents range from about 0·1 ~ 0·5 at λ = 10·6μm (see Tables 1 and 2), it is concluded that the real index causes a much larger increase (up to a factor of 3) in extinction than the imaginary index.

The Effect of Particle Size Distribution on Volume Extinction Coefficient for λ = 3·8μm and 10·6μm. The extinction σ_E is plotted as a function of geometric mean radius r_g for σ_g = 1·0, 1·5, and 2·0 for λ = 3·8μm and 10·6μm in Figures 18 and 19, respectively. The real

index was fixed at 1·8 for both wavelengths, while several realistic values of the imaginary index were chosen. The results show that extinction remains insensitive to changes in r_g up to about 0·1μm for $\sigma_g \leq 1{\cdot}5$. The optical important range shifts to a smaller size regime with increasing σ_g. The extinction decreases as $1/r_g$ for $r_g/\lambda \gtrsim 0{\cdot}25$ with the exception of k = 0·5. The extinction per unit mass decreases as $1/r_g$ for $r_g/\lambda > 0{\cdot}3$ at k = 0·5 for $\lambda \geq 3{\cdot}8\mu m$. This is in accordance with the predictions of the appendix calculations.

It is also noteworthy that r_g has the largest effect on σ_E for the lower values of k. Extinction remains constant (within a factor of about 2) with increasing values of r_g up to 1·0μm for λ = 3·8μm and 10·6μm for k = 0·5. Since typical particle size distributions of atmospheric aerosols which contribute significantly to extinction are in the range of r_g from about 0·1μm up to about 1·0μm (Table 4), the results imply that extinction is relatively independent of particle size distribution for atmospheric aerosols with large values of imaginary index (~ 0·5 or greater).

The dependence of volume absorption coefficient σ_A on r_g is discussed fully in a subsequent report [36].

DEPENDENCE OF EXTINCTION COEFFICIENT AND ABSORPTION COEFFICIENT ON WAVELENGTH AND STANDARD GEOMETRIC DEVIATION

The Effect of Wavelength λ on Extinction and Absorption Coefficients

The change in σ_E and σ_A as λ is increased from 0·55μm to 10·6μm is shown in Figure 20 for selected particle size distributions, for k = 0·01 and n = 1·7. The absorption coefficient σ_A varied as $1/\lambda$ as predicted

by Eq. (9) for $r_g/\lambda \leq 0{\cdot}05$ and $\sigma_g \leq 1{\cdot}5$.

The extinction σ_E becomes nearly constant with λ for $\lambda \leq 3{\cdot}8\mu m$ for $r_g \geq 1{\cdot}0\mu m$ and $k = 0{\cdot}01$, irrespective of the σ_g value. Some selected values of extinction and absorption coefficients at $\lambda = 0{\cdot}55\mu m$, $1{\cdot}06\mu m$, and $10{\cdot}6\mu m$ are given in Table 22 for a wide range of r_g and σ_g values.

The table shows that σ_E decreases by 2 and 3 orders of magnitude as λ increases from $0{\cdot}55\mu m$ to $10{\cdot}6\mu m$ for r_g up to about $0{\cdot}5\mu m$. For $r_g \gtrsim 0{\cdot}5\mu m$, increasing values of σ_g diminish the relative decrease of both σ_E and σ_A with λ.

These Mie results can be approximated by a power law between σ_E, σ_A, and λ:

$$\sigma_A = c\lambda^y \tag{23}$$

where the exponent y initially increases from -1 to a maximum of about -1.7 for σ_A and thereafter decreases with increasing σ_g and r_g. The parameters for various values of k and n are found in Table 23. The extinction exponent attains a maximum value of -3.5 for particles of radius $0{\cdot}1\mu m$, becomes positive at $r_g \simeq 0{\cdot}5\mu m$, and thereafter becomes constant with increasing r_g.

An increase in k from 0·01 to 0·1 causes a decrease in the exponent for extinction for $r_g = 0{\cdot}01\mu m$, $0{\cdot}1\mu m$, and $1{\cdot}0\mu m$, and a decrease in the exponent for absorption for $r_g = 0{\cdot}1\mu m$ and $1{\cdot}0\mu m$. The relative insensitivity of σ_E and σ_A to λ at large r_g/λ is a consequence of the increasing dependence of the coefficients on the geometrical cross-sectional

area of the particles.

Table 24 shows a comparison of σ_E and σ_A for particular size distributions which are generally representative of soil derived aerosols [5], at λ = 1·06μm, 3·8μm, and 10·6μm. Different values of k are assigned to the distributions at the three wavelengths and are considered to represent a range of realistic values of k for atmospheric aerosol at these wavelengths.

The ratio of σ_E (λ = 3·8)/σ_E (λ = 10·6) increases with decreasing r_g values and possesses values of about 10, 5, and 3 for r_g = 0·25, 1·0, and 0·5. Extinction at λ = 1·06μm and 3·8μm is nearly identical for r_g = 0·5μm and 1·0μm but differs by a factor of about 2·0 at r_g = 0·25. Absorption is relatively constant for the three wavelengths at r_g = 0·5μm and 1·0μm but differs by up to a factor of 5 for the lowest r_g value.

The Influence of Geometric Standard Deviation Volume Extinction and Absorption Coefficient

Figure 21 shows the effect of geometric standard deviation σ_g on σ_E for λ = 0·55μm, 1·06μm, 3·8μm, and 10·6μm, and for a range of r_g from 0·005μm up to 0·1μm. The following conclusions can be drawn:

1. σ_g has the largest effect on σ_E for $\lambda \leq$ 1·06μm and for $r_g \leq$ 0·1μm.
2. Increases in σ_E of up to an order of magnitude or greater are noted for $r_g \leq$ 0·1, as σ_g is increased from 1·0 to 2·5. For the larger particle regime, 0·25 $\leq r_g \leq$ 10μm, variation of σ_g from 1·0 to 2·0 causes a change in σ_E of not more than a factor of about 3 for the wavelengths 0·55μm, 1·06μm, 3·8μm, and 10·6μm.

CONCLUSIONS

Wavelength Range 0·55μm to 1·06μm

The ratio of volume extinction coefficient $\frac{\sigma_E\ (n = 1{\cdot}8)}{\sigma_E\ (n = 1{\cdot}33)}$ which covers the real index range for the majority of atmospheric aerosols has values up to a factor of 5 for $0{\cdot}01 \leq r_g/\lambda \leq 0{\cdot}2$ in the wavelength range 0·55μm to 1·06μm for imaginary index k = 0·005. This result is in contrast to the nearly constant value of extinction as imaginary index k is varied from 0·001 to about 0·025 at n = 1·5, 1·7 over the r_g/λ range $0{\cdot}01 < r_g/\lambda \leq 0{\cdot}2$.

The extinction coefficient becomes relatively independent of both real and imaginary index for $r_g/\lambda >$ about 0·2 over a wide range of k (0·001 to 2·0) and n (1·4 to 2·5) over a wide range of particle size distributions. Since typical particle size distributions of particles in the atmosphere possess geometric mean radii $r_g \tilde{\geq} 0{\cdot}01\mu m$, the results suggest that wide variations in the optical constants over the wavelength range 0·55μm to 1·06μm do not influence the extinction.

These results emphasize the relative insensitivity of extinction to n and k for typical particle size distributions measured, and the results should be carefully considered in connection with current and possible future measurements of optical constants in the wavelength region up to

at least 1·06μm.

The volume absorption coefficient is almost insensitive to variations in the real refractive index and independent of particle size distribution for $0{\cdot}01 \leq r_g/\lambda \leq 10$ which covers the majority of atmospheric particle size distribution values of geometric mean radius.

The absorption σ_A increases linearly with imaginary index for k values from 0·001 up to about 0·01 for $r_g/\lambda \leq 0{\cdot}5$ and $\sigma_g \leq 2{\cdot}0$. This k range for linearity of σ_A with k is narrowed for increasing r_g/λ values.

Absorption per unit mass is nearly independent of particle size distribution (within a factor of about 3) for $r_g/\lambda \lesssim 0{\cdot}75$ and $k \lesssim 0{\cdot}05$, and decreases as $1/r_g$ for $r_g/\lambda \gtrsim 7{\cdot}0$ for $k \gtrsim 0{\cdot}05$. Typical atmospheric values of k vary from about 0·005 to 0·10 for the wavelength range 0·55μm to 1·06μm.

The extinction per unit mass increases with increasing σ_g for $r_g/\lambda \lesssim 0{\cdot}5$, while the extinction decreases with increasing σ_g for $r_g/\lambda \lesssim 0{\cdot}5$, for $k \leq 0{\cdot}1$. The extinction σ_E is independent of r_g and σ_g within a factor of about 2 for $r_g/\lambda < 0{\cdot}25$ for $k = 0{\cdot}5$. In addition, $\sigma_E \simeq 1/r_g$ for $r_g/\lambda \gtrsim 0{\cdot}5$ over the range $0{\cdot}005 \leq k \leq 0{\cdot}5$.

Wavelength Range 3·8μm to 10·6μm

Variations in the real index of refraction n affects significantly the volume extinction coefficient σ_E and volume absorption coefficient σ_A for the wavelength range 3·8μm to 10·6μm. Extinction is more sensitive to n than k (up to a factor of about 3) for the majority of size

distribution parameters which well represent typically measured atmospheric aerosol values.

The extinction σ_E is well approximated by the following formula:

$$\sigma_E = \sigma_{E\,max} \exp \left\{ -\frac{1}{2} \left[\frac{(\ell n/n_g)}{\ell n\, \sigma_n} \right]^2 \right\}$$

where σ_E max is the extinction at the maximum value of $n = n_g$, where σ_n is the geometric standard deviation of σ_E distributed with respect to n. This formula holds over a wide range of r_g and σ_g for λ = 3·8μm and 10·6μm.

In the regime where extinction is linearly proportional to k, extinction σ_E can be written as

$$\sigma_E = ak \exp \left\{ -\frac{1}{2} \left[\frac{\ell n\ (n/n_g)}{\ell n\, \sigma_n} \right]^2 \right\},$$

where a is a constant.

Extinction is invariant to a relatively wide range of imaginary index 0·001 to 8·0 for $r_g/\lambda \gtrsim 0{\cdot}08$ and $\sigma_g \geq 2{\cdot}0$ and invariant for k over the same range for $r_g \gtrsim 0{\cdot}25\mu m$ and $\sigma_g > 2{\cdot}0$ for both 3·8μm and 10·6μm. The r_g/λ range above covers some of the measured aerosol size distribution geometric mean radii for $3{\cdot}8\mu m \leq \lambda \leq 10{\cdot}6\mu m$. Since the k range 0·001 to 0·5 covers most of the imaginary index values of atmospheric constituents, it is concluded that extinction is insensitive to imaginary index k for r_g values $\gtrsim$ 0·3μm and 0·8μm for 3·8μm and 10·6μm.

The particle size distribution is of major importance in determining the dependence of extinction and absorption on real index n.

The geometric mean radius r_g has the largest effect on extinction for $k \leq 0{\cdot}1$. Extinction is independent of particle size distribution, within a factor of about 2 for $r_g/\lambda \tilde{\leq} 0{\cdot}15$, $\sigma_g \tilde{\leq} 2{\cdot}0$, for $k = 0{\cdot}5$. The extinction decreases as $1/r_g$ for $r_g/\lambda > \sim 0{\cdot}25$ for $k \leq 0.5$.

The extinction is reduced by factors of 10, 5, and about 3 at $\lambda = 10{\cdot}6\mu m$ compared to 3·8 for reasonably representative values of both atmospheric particle size distributions ($r_g = 0{\cdot}25$, 1·0, and 0·5, respectively) and optical constants. For a typical range of r_g in the atmosphere $0{\cdot}25 \leq r_g \leq 10\mu m$, an increase in geometric standard deviation from 1·0 to 2·0 has relatively little influence (less than factor of about 3) on the extinction, while changes in absorption of not more than a factor of 2 are effected for $0{\cdot}005 \leq r_g \leq 10\mu m$ for the same variation in σ_g.

APPENDIX

VOLUME EXTINCTION COEFFICIENT FOR A LOGNORMAL DISTRIBUTION WITH PARTICLE RADIUS r >> WAVELENGTH λ.

$$n(r) = \frac{N}{\sqrt{2\pi}\,\ell n\,\sigma_g}\,\frac{1}{r}\,\exp\left\{-\frac{1}{2}\left[\frac{\ell n\,(r/r_g)}{\ell n\,\sigma_g}\right]^2\right\} \qquad \text{(A-1)}$$

for a Lognormal distribution

Extinction coefficient for $r >> \lambda$

$$= 2\int_0^\infty \pi r^2\, n(r)\, dr \qquad \text{(A-2)}$$

$$= \frac{2\pi N}{\sqrt{2\pi}\,\ell n\,\sigma_g}\int_0^\infty r\,\exp\left\{-\frac{1}{2}\left[\frac{\ell n\,(r/r_g)}{\ell n\,\sigma_g}\right]^2\right\}dr \qquad \text{(A-3)}$$

$$\text{Volume} = \frac{4\pi}{3}\int_0^\infty r^3\, n(r)\, dr \qquad \text{(A-4)}$$

$$= \frac{4\pi}{3}\,\frac{N}{\sqrt{2\pi}\,\ell n\,\sigma_g}\int_0^\infty r^2\,\exp\left\{-\frac{1}{2}\left[\frac{(\ell n\,(r/r_g)}{\ell n\,\sigma_g}\right]^2\right\}dr \qquad \text{(A-5)}$$

$$\frac{\text{Extinction Coefficient for } r >> \lambda}{\text{Volume}} = \frac{\frac{3}{2}\cdot\int_0^\infty r\,\exp\left\{-\frac{1}{2}\left[\frac{\ell n(r/r_g)}{\ell n\,\sigma_g}\right]^2\right\}dr}{\int_0^\infty r^2\,\exp\left\{-\frac{1}{2}\left[\frac{\ell n\,r/r_g}{\ell n\,\sigma_g}\right]^2\right\}dr} \qquad \text{(A-6)}$$

Examine

$$\int_0^\infty r\,\exp\left\{-\frac{1}{2}\left[\frac{\ell n\,(r/r_g)}{\ell n\,\sigma_g}\right]^2\right\}dr \qquad \text{(A-7)}$$

This has the form

$$\int_0^\infty r\,\exp\,(-k\;\ell n^2\;cr)\,dr$$

$$\text{where } k = \frac{1}{2\;\ell n^2\sigma_g} \text{ and } c = \frac{1}{r_g} \qquad \text{(A-8)}$$

Let $y = \ell n\ cr$

$$\therefore r = \frac{\exp y}{c} \qquad \text{and } dr = \frac{\exp (y)\ dy}{c} \tag{A-9}$$

Therefore Eq. (A-7) becomes

$$\frac{1}{c^2} \int_{-\infty}^{+\infty} \exp (2y) \exp (-ky^2)\, dy \tag{A-10}$$

According to Gradshteyn and Ryzhik [44], integrals of the form

$$\int_{-\infty}^{+\infty} \exp\ (-p^2\ y^2 + qy)\, dy$$

have a solution equal to

$$\exp \left(\frac{q^2}{4p^2}\right) \cdot \frac{\sqrt{\pi}}{p} \quad \text{for } p > 0$$

Therefore, Eq. (A-10) reduces to

$$r_g^2 \cdot \sqrt{2\pi}\ \ell n\ \sigma_g\ \exp\ (2\ \ell n^2\ \sigma_g) \tag{A-11}$$

We now consider

$$\int_0^{\infty} r^2\ \exp \left\{-\frac{1}{2}\left[\frac{\ell n\ r/r_g}{\ell n\ \sigma g}\right]^2\right\} dr \tag{A-12}$$

This expression is written as

$$\int_0^{\infty} r^2\ \exp\ [-k\ \ell n^2\ cr]\, dr$$

using the same constants as in (A-8).

Eq. (A-12) reduces to

$$\frac{1}{c^3} \int_{-\infty}^{\infty} \exp\ (3y) \exp\ (-ky^2)\, dy \tag{A-13}$$

which is reducible to the following form:

$$r_g^3\ \sqrt{2\pi}\ \ell n\ \sigma_g\ \exp\ (4{\cdot}5\ \ell n^2\ \sigma_g) \tag{A-14}$$

using the integral solution of [39].

Therefore the expression for $\frac{\text{extinction coefficient for } r >> \lambda}{\text{volume of distribution}}$

is equal to

$$\frac{3}{2} \cdot \frac{1}{r_g} \exp\left(-2.5 \ln^2 \sigma_g\right) \qquad \text{(A-15)}$$

TABLE 1. REAL AND IMAGINARY PART OF THE COMPLEX REFRACTIVE INDEX OF SEVERAL ATMOSPHERIC CONSTITUENTS

Constituent	Refractive Index	Wavelength 0.55μm to 1.06μm	3.0μm to 5.0μm	9.0μm to 11.0μm
$(NH_4)_2\ SO_4$ [ref 12] (crystalline form)	n*	1.52 to 1.55	1.27 to 1.63	0.99 to 2.86
	k**	Upper limit of 1×10^{-7}	0.006 to 0.33	0.02 to 2.1
$(NH_4)_2\ SO_4$ [ref 13] 3.2 m solution	n	-	1.2 to 1.5	1.3 to 1.65
	k	-	0.0 to 0.24	0.06 to 0.56
NaCl [ref 12] (crystalline)	n	1.53 to 1.55	1.52 to 1.51	1.49 to 1.50
	k	Upper limit of 1×10^{-7}	Upper limit of 1×10^{-7}	1.0×10^{-7} to 1.9×10^{-7}
NaCl [ref 14] 0.25 m solution	n	Not given	1.325 to 1.475	1.156 to 1.263
	k	Not given	0.004 to 0.268	0.04 to 0.093
NaCl 0.5 m solution	n	Not given	1.327 to 1.481	1.162 to 1.265
	k	Not given	0.000 to 0.262	0.039 to 0.091
H_2O [ref 15]	n	1.327 to 1.335	1.325 to 1.483	1.153 to 1.262
	k	1.0×10^{-9} to 3.48×10^{-6}	0.003 to 0.272	0.04 to 0.097
Quartz [ref 16] (crystalline)	n	1.539	1.412 to 1.48	0.11 to 6.38
Ordinary ray	k	-	0.00001 to 0.00079	0.017 to 7.51
Extraordinary ray	n	1.584	Not given	0.11 to 7.51
	k	-	Not given	0.015 to 6.37
25% solution of H_2SO_4 in water [ref 18]	n	1.359 to 1.366	1.324 to 1.431	1.346 to 1.442
	k	3.02×10^{-8} to 2.75×10^{-6}	0.028 to 0.193	0.151 to 0.273
50% solution of H_2SO_4 in water [ref 18]	n	1.389 to 1.397	1.329 to 1.379	1.433 to 1.650
	k	2.07×10^{-8} to 2.09×10^{-6}	0.076 to 0.141	0.199 to 0.463
75% solution of H_2SO_4 in water [ref 18]	n	1.422 to 1.431	1.294 to 1.405	1.589 to 1.947
	k	2.07×10^{-8} to 1.53×10^{-6}	0.099 to 9.161	0.271 to 0.711
Carbon [19, 20, 21, 22] coals and soots	n	1.5 to 2.1	1.55 to 2.0	2.0 to 2.45
	k	0.015 to 0.65	0.25 to 0.8	0.35 to 1.2
20% solution of ZnCl in water [ref 23]	n	Not given	1.365 to 1.491	1.207 to 1.302
	k	Not given	0.012 to 0.256	0.048 to 0.095
30% solution of ZnCl in water [ref 23]	n	Not given	1.377 to 1.497	1.232 to 1.320
	k	Not given	0.004 to 0.226	0.041 to 0.092
40% solution of ZnCl in water [ref 23]	n	Not given	1.402 to 1.506	1.265 to 1.344
	k	Not given	0.010 to 0.200	0.042 to 0.088
Limestone [ref 24]	n	1.550 to 1.569	1.467 to 1.543	1.545 to 1.723
	k	0.025 to 0.052	0.045 to 0.068	0.169 to 0.201
Montmorillite [ref 25]	n	Not evaluated	1.37 to 1.42 (at 5.0μm)	0.71 to 2.78
	k	Not evaluated	0.004 to 0.005 (at 5.0μm)	0.15 to 2.06

*n = real index.
**k = imaginary index.

TABLE 2. REAL AND IMAGINARY PART OF THE COMPLEX INDEX OF REFRACTION OF ATMOSPHERIC PARTICLES, DUST, AND MARINE AEROSOL.

Constituent	Refractive Index	Wavelength 0.55μm to 1.06μm	Wavelength 3.0μm to 5.0μm	Wavelength 9.0μm to 11.0μm
Urban air density = 2.7 g cm^{-3}[ref 26]	n*	Not given	Not measured	Not measured
	k**	0.0049-0.008	Not measured	Not measured
Maritime air density = 2.4 g cm^{-3}[ref 26]	n	Not measured	Not measured	Not measured
	k	0.00033-0.0011	Not measured	Not measured
Desert aerosol [ref 28]	n	Not measured	Not measured	Not measured
	k	0.004-0.10	Not measured	Not measured
Urban aerosol [ref 10]	n	1.485-1.66	Not measured	Not measured
	k	Not measured	Not measured	Not measured
Urban aerosol density = 2.7 g cm^{-3} [ref 27]	n	Not measured	No measurement	Not measured
	k	Not measured	0.104-0.131	0.139-0.365
Marine aerosol density = 2.4 gm^{-3} [ref 27]	n	Not measured	No measurement	Not measured
	k	Not measured	0.075-0.086	0.052-0.081
Desert aerosol assumed density 2.5 gm^{-3} [ref 27]	n	Not measured	No measurement	Not measured
	k	Not measured	0.028-0.13	0.0025-0.375

* n = real index

** k = imaginary index

TABLE 3. RANGE OF MEASURED OPTICAL CONSTANTS OF SEVERAL ATMOSPHERIC CONSTITUENTS

(Ammonium Sulfate, Sodium Chloride, Water, Sulfuric Acid Solutions, Acid and Oil Smokes, Carbon, Quartz, and Atmospheric Dust)

Wavelength Range (μm)	Real Index	Imaginary Index
0·55 to 1·0	1·32 to 2·1	0 to 0·8
3·0 to 5·0	1·2 to 3·1	0 to 1·35
9·0 to 11·0	0·11 to 7·51	0 to 7·51

TABLE 4. TYPICAL LOGNORMAL PARAMETERS FOR MEASURED ATMOSPHERIC AEROSOL POLYDISPERSIONS

Types of Atmospheric Aerosol	Lognormal Component	Geometric Mean Radius (μm)	Geometric Standard Deviation
Heavy aerosol	1	0·47	2·2
(mass ~ $10^4 \mu gm^{-3}$) [ref 7]	2	26·0	1·37
Moderate aerosol	1	0·12	2·41
(mass ≃ $10^3 \mu gm^{-3}$) [ref 7]	2	8·0	2·0
Light aerosol	1	0·03	2·4
(mass ≃ $10^2 \mu gm^{-3}$) [ref 33]	2	1·6	1·6
Fog	1	0·25	2·1
(mass ≃ 5 x $10^5 \mu gm^{-3}$) [ref 34]	2	4·5	1·65
Heavy Fog	1	0·5	2·5
(mass ≃ $10^6 \mu gm^{-3}$) [ref 34]	2	4·5	1·8
Aerosol measured	1	0·375	1·25
from aircraft	2	0·77	1·5
altitude ≤ 5 km	3	2·85	1·25
(mass ≃ $50 \mu gm^{-3}$) [ref 35]	4	3·75	1·5
Maritime aerosol	1	0·05	1·4
(mass ≃ $30 \mu gm^{-3}$) [ref 36]	2	0·133	1·4
	3	0·44	1·7
	4	1·50	1·7
	5	9·0	1·6

TABLE 5. PARTICLE SIZE DISTRIBUTION PARAMETERS USED IN THE PLOTS OF EXTINCTION AND ABSORPTION COEFFICIENTS, WITH REAL INDEX n (FIGURES 1 TO 8) FOR IMAGINARY INDEX k = 0·01

Wavelength λ(μm)	Geometric Mean Radius r_g (μm)	Geometric Standard Deviation σ_g
0·55	0·005	1·0
0·55	0·005	2·0
0·55	0·005	2·5
0·55, 1·06	0·01	1·25
0·55, 1·06	0·01	2·0
0·55, 1·06	0·01	2·5
0·55, 1·06	0·05	1·0
0·55, 1·06	0·05	1·5
0·55, 1·06	0·05	2·0
0·55, 1·06	0·05	2·5
0·55, 1·06	0·1	1·0
0·55, 1·06	0·1	1·5
0·55, 1·06	0·1	2·0
0·55	0·25	1·0
0·55	0·25	1·5
0·55	0·25	2·0
0·55, 1·06	0·5	1·0
0·55, 1·06	0·5	2·0
0·55	0·75	1·0
0·55	0·75	1·5
0·55, 1·06	1·0	1·0
0·05, 1·06	1·0	1·5
0·55	2·5	1·0
0·55	2·5	1·5
0·55, 1·06	5·0	1·0
0·55, 1·06	5·0	1·5

TABLE 6. THE RATIO OF EXTINCTION COEFFICIENTS σ_E (n)/σ_E (n = 1.33) AS A FUNCTION OF n, r_g/λ AND σ_g; IMAGINARY INDEX k = 0.005

	σ_E (n)/σ_E (n = 1.33)													
	r_g/λ = 0.01				r_g/λ = 0.02			r_g/λ = 0.1				r_g/λ = 0.2		
n/σ_g	1.0	1.5*	2.0*	2.5*	1.125	2.0*	2.5*	1.0	1.5*	2.0*	2.5*	1.0	1.5*	2.0*
1.33	1.0	1.0	1.0	1.0	1.0	1.0	1.0	1.0	1.0	1.0	1.0	1.0	1.0	1.0
1.4	0.955	0.959	1.058	1.389	0.962	1.284	1.42	1.259	1.410	1.349	1.130	1.426	1.458	1.169
1.5	0.890	0.902	1.161	2.086	0.913	1.77	2.11	1.694	2.136	1.824	1.271	2.167	2.191	1.351
1.6	0.826	0.835	1.282	2.967	0.857	2.35	2.82	2.194	3.038	2.234	1.369	3.056	3.008	1.475
1.7	0.765	0.795	1.418	4.035	0.803	3.00	3.60	2.744	4.137	2.590	1.440	4.083	3.789	1.553
1.8	0.708	0.744	1.565	5.382	0.769	3.72	4.16	3.331	5.440	2.863	1.490	5.250	4.510	1.604

*Combinations of values of σ_g and n that are representative of atmospheric aerosols are indicated by an asterisk.

The above values were caluclated at λ = 0.55μm. However, subsequent calculations have shown the values to be within 12% of those values for 0.55μm $\leq \lambda \leq$ 1.06μm.

TABLE 7. RANGE OF IMAGINARY INDEX, k, FOR WHICH THE VOLUME EXTINCTION COEFFICIENT IS CONSTANT TO WITHIN ABOUT 20% OR LESS

r_g/λ*	Imaginary Index	Geometric Standard Deviation σ_g
0.01	0.001-0.0025 (λ = 10.6μm only)	2.0
0.01	0.001-0.01	2.0
0.01	0.001-0.02	2.5
0.05	0.001-0.005	1.5
0.05	0.001-0.025	2.0
0.05	0.001-0.1 (λ = 10.6μm only)	2.0
0.01	0.001-0.05	1.5
0.01	0.001-0.3	2.0
0.25	0.001-0.1	1.5
0.25	0.001-0.25	2.0
0.5	0.001-6.0+	1.5
0.5	0.001-6.0+	2.0
1.0	0.001-6.0+	1.5
1.0	0.001-6.0+	2.0

*Applicable to wavelengths 0.55, 0.694, 1.06, 3.8 and 10.6 micrometers.
+The upper limit of the imaginary index is only realistic at 10.6μm wavelength.

TABLE 8. VALUES OF IMAGINARY INDEX k_ℓ BELOW WHERE THE ABSORPTION COEFFICIENT VARIES LINEARLY (WITHIN 20%) WITH IMAGINARY INDEX k WAVELENGTH = 0·55μm; REAL INDEX = 1·55

Geometric Mean Radius r_g(μm)	Geometric Standard Deviation σ_g	k_ℓ
0·1	1·5	0·1
0·1	2·0	0·025
0·1	2·5	0·01
0·1	3·0	0·005
0·25	1·5	0·025
0·25	2·0	0·01
0·25	2·5	0·005
0·25	3·0	0·001
0·5	1·5	0·01
0·5	2·0	0·005
0·5	2·5	0·0025
1·0	1·5	0·005
1·0	2·0	0·0025
1·0	2·25	0·001

TABLE 9. VALUES OF IMAGINARY INDEX k_ℓ BELOW WHERE THE ABSORPTION COEFFICIENT VARIES LINEARLY (WITHIN 20%) WITH IMAGINARY INDEX k
WAVELENGTH = 1·06μm; REAL INDEX = 1·6

Geometric Mean Radius $r_g(\mu m)$	Geometric Standard Deviation σ_g	k_ℓ
0·1	1·5	0·5
0·1	2·0	0·05
0·1	2·5	0·01
0·1	3·0	0·005
0·25	1·5	0·10
0·25	2·0	0·025
0·25	2·5	0·01
0·25	3·0	0·0025
0·5	1·5	0·025
0·5	2·0	0·01
0·5	2·5	0·005
1·0	1·5	0·005
1·0	2·0	0·005
1·0	2·25	0·001

TABLE 10. VALUES OF IMAGINARY INDEX k_c, ABOVE WHICH THE ABSORPTION COEFFICIENT IS CONSTANT (TO WITHIN ABOUT 40%) WITH IMAGINARY INDEX WAVELENGTH = 0·55μm; REAL INDEX = 1·55

Geometric Mean Radius r_g (μm)	Geometric Standard Deviation σ_g	k_c
0·1	1·5	0·25
0·1	2·0	0·25
0·1	2·5	0·1
0·1	3·0	0·05
0·25	1·5	0·10
0·25	2·0	0·05
0·25	2·5	0·025
0·25	3·0	0·025
0·5	1·5	0·05
0·5	2·0	0·025
0·5	2·5	0·025
1·0	1·5	0·025
1·0	2·0	0·025
1·0	2·25	0·01

TABLE 11. VALUES OF IMAGINARY INDEX k_c ABOVE WHICH THE ABSORPTION COEFFICIENT IS CONSTANT (TO WITHIN ABOUT 40%) WITH IMAGINARY INDEX. WAVELENGTH = 1·06μm; REAL INDEX = 1·6

Geometric Mean Radius r_g(μm)	Geometric Standard Deviation (σ_g)	k_c
0·1	1·5	1·0
0·1	2·0	0·5
0·1	2·5	0·1
0·1	3·0	0·05
0·25	1·5	0·25
0·25	2·0	0·10
0·25	2·5	0·05
0·25	3·0	0·025
0·5	1·5	0·1
0·5	2·0	0·05
0·5	2·5	0·025
1·0	1·5	0·05
1·0	2·0	0·025
1·0	2·25	0·025

TABLE 12. VALUES OF n_g*, σ_n+ WHICH SATISFY THE EQUATION

$$\sigma_E = \sigma_{Emax} \text{ EXP } \left\{ -\frac{1}{2} \left[\frac{\ell n(n/n_g)}{\ell n\ \sigma_n} \right]^2 \right\} \text{ FOR A}$$

SELECTION OF r_g, σ_g, AND k VALUES AT λ = 3.8μm

λ	r_g	σ_g	n_g	σ_n	σ_{Emax}	k
3.8	0.05	1.5	0.8	2.25	6.34×10^{-3}	0.05
3.8	0.05	2.5	5.5	2.15	9.0×10^{-2}	0.05
3.8	0.1	2.0	6.0	1.925	1.1×10^{-1}	0.01
3.8	0.1	2.0	6.0	1.925	1.1×10^{-1}	0.05
3.8	0.5	2.0	2.6	1.9	5.2×10^{-2}	0.05
3.8	1.0	1.5	2.1	1.43	6.64×10^{-2}	0.05

* Peak extinction occurs at real index n = n_g

+ σ_n is the geometric standard deviation of the n values centered around n_g.

TABLE 13. RANGE OF IMAGINARY INDEX k, FOR WHICH THE EXTINCTION COEFFICIENT IS CONSTANT (TO WITHIN 15%). WAVELENGTH = 3·8μm; REAL INDEX n = 1·7

Range of k for Which Extinction is Constant	Geometric Mean Radius, r_g	Geometric Standard Deviation, σ_g
0·001 to 0·005	0·05	2·0
0·001 to 0·05	0·05	2·5
0·001 to 0·025	0·1	2·0
0·001 to 0·015	0·25	1·5
0·001 to 0·25	0·25	2·0
0·001 to 0·1	0·5	1·5
0·001 to 2·0	0·5	2·0
0·001 to 1·0	0·75	1·5
0·001 to 2·0	0·75	2·0
0·001 to 2·0	$r_g \geq 1·0$	$\sigma_g \geq 1·5$

TABLE 14. THE RATIO OF EXTINCTION COEFFICIENTS AT VALUES OF REAL INDEX n, σ_E (n)/σ_E (n = 1·4), FOR TYPICAL AEROSOL SIZE DISTRIBUTIONS. WAVELENGTH λ = 3·8μm; IMAGINARY INDEX k = 0·025

σ_E (n)/σ_E (n = 1·4)

n \ σ_g	r_g = 0·01 μm		r_g = 0·05 μm			r_g = 0·1 μm			r_g = 0·25 μm			r_g = 0·5 μm			r_g = 1·0 μm		
	2·0	2·5	1·5	2·0	2·5	1·5	2·0	2·5	1·5	2·0	2·5	1·5	1·75	2·0	1·5	1·75	2·0
1·4	1·0	1·0	1·0	1·0	1·0	1·0	1·0	1·0	1·0	1·0	1·0	1·0	1·0	1·0	1·0	1·0	1·0
1·6	0·86	0·93	0·87	1·12	1·88	0·96	1·68	1·64	1·55	1·80	1·30	2·0	1·76	1·40	1·64	1·27	1·12
1·8	0·74	0·86	0·77	1·29	2·93	0·94	2·69	2·14	2·28	2·53	1·48	3·3	2·37	1·64	1·99	1·36	1·14
2·0	0·63	0·85	0·67	1·49	3·96	0·94	3·99	2·54	3·18	3·08	1·59	4·65	2·78	1·77	2·09	1·36	1·14
2·25	0·52	0·83	0·57	1·77	5·03	0·95	5·79	2·93	4·72	3·60	1·66	6·13	3·09	1·84	2·04	1·33	1·11
2·5	0·43	0·82	0·49	2·07	5·84	0·98	7·67	3·19	7·02	3·97	1·69	7·13	3·24	1·86	1·92	1·29	1·09

TABLE 15. RANGE OF IMAGINARY INDEX k FOR WHICH EXTINCTION COEFFICIENT IS LINEAR (TO WITHIN 10%) WITH k; n = 1·7, λ = 3·8μm

Range of k, for Which σ_E is Linear with k	r_g	σ_g
0·001 to 1·0	0·01	$\leq$ 2·0
0·025 to 1·0	0·01	2·5
0·001 to 1·0	0·05	1·0*
0·01 to 1·0	0·05	1·5
0·05 to 1·0	0·05	2·0
0·01 to 1·0	0·1	1·0*
0·05 to 1·0	0·1	1·5
0·25 to 1·0	0·1	2·0
0·25 to 1·0	0·5	$\leq$ 1·125*

*Values of σ_g do not represent realistic values for atmospheric aerosols.

TABLE 16. PARTICLE SIZE DISTRIBUTION PARAMETERS USED IN THE VOLUME EXTINCTION COEFFICIENT VERSUS REAL INDEX OF REFRACTION AT λ = 10·6μm (Figures 12-14).

Geometric Mean Radius r_g	Geometric Standard Deviation σ_g	Geometric Mean Radius r_g	Geometric Standard Deviation σ_g
0·005	1·0	0·5	1·0
0·005	1·5	0·5	2·0
0·005	2·0		
0·005	2·5	0·75	1·0
		0·75	1·5
0·01	1·0		
0·01	2·0	1·0	1·0
0·01	2·5	1·0	1·5
0·05	1·0	2·5	1·0
0·05	1·5	2·5	1·5
0·05	2·0		
0·05	2·5	5·0	1·0
		5·0	1·5
0·1	1·0		
0·1	2·0	10·0	1·0
		10·0	1·5
0·25	1·0		
0·25	1·5		
0·25	2·0		

TABLE 17. VALUES OF n_g, σ_g, WHICH SATISFY THE EQUATION

$$\sigma_E = \sigma_{Emax} \exp \left\{ -\frac{1}{2} \left[\frac{\ell n\ (n/n_g)}{\ell n\ \sigma_n} \right]^2 \right\}$$

FOR A SELECTION OF r_g, σ_g AND k VALUES AT λ = 10·6μm

λ	r_g	σ_g	n_g	σ_{Emax}	σ_n	k
10·6	0·05	2·0	0·8	$4·38 \times 10^{-3}$	2·25	0·1
10·6	0·10	2·0	0·8	$4·33 \times 10^{-3}$	2·5	0·1
10·6	0·25	2·0	6·5	$3·73 \times 10^{-3}$	1·9	0·1
10·6	0·5	2·0	4·35	$3·7 \times 10^{-3}$	2·1	0·1
10·6	0·75	1·5	5·0	$5·27 \times 10^{-3}$	1·625	0·01
10·6	0·75	1·5	5·0	$5·27 \times 10^{-3}$	1·65	0·1
10·6	1·0	1·5	4·2	$5·6 \times 10^{-3}$	1·65	0·1
10·6	2·5	1·5	2·25	$2·62 \times 10^{-3}$	1·5	0·1

TABLE 18. VALUES OF THE RATIO OF EXTINCTION COEFFICIENTS σ_E (n)/σ_E (n = 1·2) AT WAVELENGTH λ = 10·6μm FOR TYPICAL AEROSOL SIZE DISTRIBUTIONS. IMAGINARY INDEX k = 0·05

σ_E (n)/σ_E (n = 1·2)

n \ σ_g	r_g = 0·1 μm			r_g = 0·25 μm			r_g = 0·5 μm			r_g = 0·75 μm			r_g = 1·0 μm			r_g = 2·5 μm		
	1·5	2·0	2·5	1·5	2·0	2·5	1·5	2·0	2·5	1·5	2·0	2·5	1·5	2·0	2·5	1·5	2·0	2·5
1·2	1·0	1·0	1·0	1·0	1·0	1·0	1·0	1·0	1·0	1·0	1·0	1·0	1·0	1·0	1·0	1·0	1·0	1·0
1·4	0·88	0·93	1·42	0·91	1·28	2·10	1·07	1·93	1·94	1·33	2·19	1·73	1·63	2·21	1·59	2·4	1·63	1·22
1·6	0·76	0·86	2·15	0·83	1·74	3·37	1·19	3·34	2·66	1·88	3·64	2·19	2·68	3·38	1·91	3·99	1·89	1·27
1·8	0·65	0·80	3·18	0·75	2·42	4·43	1·36	4·96	3·17	2·61	4·90	2·47	4·20	4·24	2·08	5·12	1·97	1·28
2·0	0·55	0·76	4·37	0·69	3·36	5·29	1·57	6·49	3·53	3·58	5·87	2·63	6·08	4·86	2·16	5·64	1·98	1·27
2·25	0·45	0·73	6·0	0·63	4·86	6·15	1·87	8·03	3·80	5·30	6·78	2·74	8·77	5·33	2·21	5·74	1·96	1·25
2·5	0·37	0·72	7·47	0·59	6·43	6·76	2·20	9·18	3·95	7·46	7·37	2·79	11·59	5·58	2·21	5·54	1·92	1·28
3·5	0·18	0·74	10·85	0·51	11·56	8·11	6·01	11·60	4·08	16·45	8·05	2·75	18·07	5·65	2·15	4·64	1·78	1·18

TABLE 19. RANGE OF IMAGINARY INDEX k, FOR WHICH THE VOLUME EXTINCTION COEFFICIENT IS CONSTANT (TO WITHIN 15%) FOR REAL INDEX n = 1·8, WAVELENGTH λ = 10·6μm

Range of k for Which Extinction is Constant	Geometric Mean Radius r_g	Geometric Standard Deviation σ_g
0·001 to 0·0025	0·1	2·0
0·001 to 0·035	0·1	2·5
0·001 to 0·025	0·25	2·0
0·001 to 0·25	0·25	2·5
0·001 to 0·01	0·5	1·5
0·001 to 0·1	0·5	2·0
0·001 to 1·0	0·5	2·5
0·001 to 0·025	0·75	1·5
0·001 to 0·5	0·75	2·0
0·001 to 8·0	0·75	2·5
0·001 to 0·05	1·0	1·5
0·001 to 1·0	1·0	2·0
0·001 to 8·0	1·0	2·5
0·001 to 1·0	2·5	$\leq$ 1·5
0·001 to 8·0	$r_g > 2·5$	$\sigma_g \geq$ 1·0

TABLE 20. RANGE OF IMAGINARY INDEX k FOR WHICH EXTINCTION COEFFICIENT IS LINEAR WITHIN 15%, WITH k; FOR n = 1·8 λ = 10·6μm. THE SIZE DISTRIBUTION REPRESENT REALISTIC VALUES FOR ATMOSPHERIC AEROSOLS

Range of k, Over Which σ_E is Linear with k	r_g (μm)	σ_g
0·001 to 1·0	0·01	$\leq$ 2·5
0·001 to 1·0	0·05	$\leq$ 1·5
0·01 to 1·0	0·05	2·0
0·01 to 1·0	0·05	2·5
0·001 to 1·0	0·1	1·5
0·05 to 1·0	0·1	2·0
* * *	0·1	2·5
0·025 to 1·0	0·25	1·5
0·25 to 1·0	0·25	2·0
* * *	0·25	2·5
0·25 to 1·0	0·5	1·5
* * *	0·5	2·0
* * *	0·5	2·5
0·25 to 1·0	0·75	1·5
* * *	0·75	2·0
* * *	0·75	2·5
* * *	1·0	1·5
* * *	1·0	2·0
* * *	$r_g > 1·0$	$\sigma_g > 1·5$

* * *Denotes the range of k, 0·001 $\leq$ k $\leq$ 8·0 over which σ_E is not linear with k.

TABLE 21. THE RELATIVE SENSITIVITY OF THE EXTINCTION COEFFICIENT TO CHANGES IN REAL INDEX n AND IMAGINARY INDEX k AT WAVELENGTH λ = 10.6μm

Geometric Mean Radius r_g (μm)	Geometric Standard Deviation σ_g					
	Extinction Dependence on k (n = 1.8)			Extinction at n = 2.5 / Extinction at n = 1.25		
	1.5	2.0	2.5	1.5	2.0	2.5
0.1	linear for k > 0.001	linear for k > 0.05	constant (within 15%) for k: 0.001-0.25	0.38	0.48	1.93
0.25	linear for k: 0.05-1.0	constant (within 15%) for k: 0.001-0.025 linear over k: 0.25-1.0	constant for k: 0.001-0.25	0.44	1.73	2.36
0.5	constant (within 15%) for k: 0.001-0.01	constant for k: 0.001-0.1	constant for k: 0.001-1.0	0.90	2.64	2.04
0.75	constant (within 15%) for k: 0.001-0.025	constant for k: 0.001-0.5	constant for k: 0.001-8.0	2.05	2.57	1.77
1.0	constant (within 15%) for k: 0.001-0.05	constant for k: 0.001-1.0	constant for k: 0.001-8.0	2.95	2.33	1.59

TABLE 22. VALUES OF EXTINCTION COEFFICIENT σ_E AND ABSORPTION σ_A IN km^{-1} (FOR PARTICULATE MASS OF 100$\mu g/m^3$) AT λ = 0.55μm, 1.06μm, AND 10.6μm; k = 0.01, n = 1.7 FOR A RANGE OF VALUES r_g AND σ_g

r = 0.01μm

σ_g	1.125*		2.0		2.5			
λ(μm)	σ_E	σ_A	σ_E	σ_A	σ_E	σ_A	σ_E	σ_A
0.55	5.835×10^{-2}	5.60×10^{-3}	3.526×10^{-2}	6.425×10^{-3}	2.265×10^{-1}	1.10×10^{-2}		
1.06	2.903×10^{-3}	2.88×10^{-3}	4.973×10^{-3}	2.88×10^{-3}	4.92×10^{-2}	4.0×10^{-3}		
10.6	2.87×10^{-4}	2.87×10^{-4}	2.71×10^{-4}	2.71×10^{-4}	2.64×10^{-4}	2.59×10^{-4}		

r = 0.05μm

	1.0*		1.125*		1.5		2.0	
0.55	3.28×10^{-2}	6.9×10^{-3}	3.72×10^{-2}	7.07×10^{-3}	1.426×10^{-1}	9.59×10^{-3}	3.25×10^{-1}	1.535×10^{-2}
1.06	4.83×10^{-3}	3.06×10^{-3}	5.19×10^{-3}	3.09×10^{-3}	1.48×10^{-2}	3.40×10^{-3}	1.2×10^{-1}	5.8×10^{-3}
10.6	2.86×10^{-4}	2.87×10^{-4}	2.88×10^{-4}	2.88×10^{-4}	2.84×10^{-4}	2.83×10^{-4}	3.0×10^{-4}	2.75×10^{-4}

r = 0.1μm

	1.125*		1.5		2.0	
0.55	2.16×10^{-1}	1.13×10^{-2}	4.0×10^{-1}	1.56×10^{-2}	2.45×10^{-1}	1.67×10^{-2}
1.06	2.17×10^{-2}	3.73×10^{-3}	8.06×10^{-2}	5.14×10^{-3}	1.69×10^{-1}	8.07×10^{-3}
10.6	2.90×10^{-4}	2.89×10^{-4}	2.93×10^{-4}	2.85×10^{-4}	4.97×10^{-4}	2.88×10^{-4}

r = 0.5μm

	1.0*		1.125*		1.5	
0.55	1.02×10^{-1}	1.67×10^{-2}	1.19×10^{-1}	1.86×10^{-2}	4.0×10^{-2}	9.23×10^{-3}
1.06	2.36×10^{-2}	9.8×10^{-3}	2.35×10^{-1}	9.9×10^{-3}	4.56×10^{-2}	6.62×10^{-3}
10.6	4.83×10^{-4}	3.06×10^{-4}	5.19×10^{-4}	3.09×10^{-4}	1.2×10^{-2}	5.85×10^{-4}

r = 1.0μm

	1.125*		1.5	
0.55	6.6×10^{-2}	1.27×10^{-2}	4.39×10^{-2}	1.02×10^{-2}
1.06	6.18×10^{-2}	9.53×10^{-3}	4.66×10^{-2}	7.53×10^{-3}
10.5	2.12×10^{-3}	3.73×10^{-4}	8.06×10^{-3}	5.14×10^{-4}

r = 5.0μm

	1.125*		1.5	
0.55	1.17×10^{-2}	4.71×10^{-3}	8.0×10^{-3}	3.33×10^{-3}
1.06	1.21×10^{-2}	3.92×10^{-3}	8.19×10^{-3}	2.94×10^{-3}
10.6	2.35×10^{-2}	9.9×10^{-4}	1.21×10^{-2}	9.52×10^{-4}

r = 10.0μm

	1.125*		1.5	
0.55	5.73×10^{-3}	2.50×10^{-3}	3.91×10^{-3}	1.71×10^{-3}
1.06	5.85×10^{-3}	2.37×10^{-3}	3.98×10^{-3}	1.67×10^{-3}
10.6	6.18×10^{-3}	9.53×10^{-3}	4.66×10^{-4}	1.21×10^{-3}

*Appropriate for monodisperse or near monodisperse aerosol size distributions only.

TABLE 23. VARIATION OF EXTINCTION COEFFICIENT AND ABSORPTION COEFFICIENT σ_E, σ_A WITH WAVELENGTH IN THE FORM OF σ_E, $\sigma_A \sim \lambda^y$.

		Values of y					
		Wavelength Range (μm)					
r_g	σ_g	0.55 - 1.06		1.06 - 10.6		0.55 - 10.6	
		Extinction	Absorption	Extinction	Absorption	Extinction	Absorption
(i) n = 1.7, k = 0.01							
0.01	1.125	-1.06	-1.0	-1.0	-1.0	-	-1.26
0.01	2.0	-2.98	-1.22	-1.26	-1.03	-	-1.26
0.01	2.5	-2.32	-1.19	-2.27	-1.19	-	-1.26
0.1	1.125	-3.50	-1.69	No slope		No slope	
0.1	1.5	-2.44	-1.69				
0.1	2.0	-0.57	-1.10				
0.5	1.125	+1.0	-0.96	-	-1.51	No slope	
0.5	2.0	+0.2	-0.50	-	-		
1.0	1.125	-0.1	-0.44	No slope		No slope	
	1.5	+0.09	-0.46				
5.0	1.125	+0.05	-0.28	No slope		No slope	
	1.5	+0.03	-0.19				
10.0	1.125	+0.03	-0.07	0.08	-	0.03	
	1.5	0.0	0.0	-	-	-	
(ii) n = 1.8, k = 0.1							
0.01	1.125	-1.02	-1.01	-1.0	-1.0	-	-1.00
	2.0	-1.81	-1.24	-1.07	-1.03	-	-1.08
	2.5	-1.81	-1.37	-1.56	-1.19	-	-1.22
0.1	1.125	-2.79	-1.75	-1.33	-1.12	No slope	
	1.5	-1.87	-1.44	-	-	No slope	
	2.0	-0.42	-0.64	-1.80	-1.31	No slope	
1.0	1.125	+0.13	+0.12	No slope		No slope	
	1.5	+0.10	+0.14	No slope		No slope	
10.0	1.125	+0.03	+0.05	0.09	0.12	0.07	0.11
	1.5	+0.02	+0.04	0.07	0.11	0.06	0.09

TABLE 24. A COMPARISON OF σ_E AND σ_A AT λ = 1·06μm, 3·8μm AND 10·6μm FOR REALISTIC VALUES OF r_g, σ_g AND k FOR ATMOSPHERIC AEROSOLS

k	n	r_g	σ_g	λ	σ_E	σ_A
0·01	1·7	0·5	2·0	1·06	$4·56 \times 10^{-2}$	$6·62 \times 10^{-3}$
0·025	1·8	0·5	2·0	3·8	$4·59 \times 10^{-2}$	$5·67 \times 10^{-3}$
0·05	1·8	0·5	2·0	10·6	$1·54 \times 10^{-2}$	$2·83 \times 10^{-3}$
0·005	1·7	0·5	2·0	1·06	$4·56 \times 10^{-2}$	$3·84 \times 10^{-3}$
0·01	1·8	0·5	2·0	3·8	$4·62 \times 10^{-2}$	$2·60 \times 10^{-3}$
0·025	1·8	0·5	2·0	10·6	$1·50 \times 10^{-2}$	$1·51 \times 10^{-3}$
0·01	1·7	0·5	2·0	1·06	$4·56 \times 10^{-2}$	$6·62 \times 10^{-3}$
0·05	1·8	0·5	2·0	3·8	$4·54 \times 10^{-2}$	$9·44 \times 10^{-3}$
0·25	1·8	0·5	2·0	10·6	$1·87 \times 10^{-2}$	$9·85 \times 10^{-3}$
0·005	1·7	1·0	1·5	1·06	$4·65 \times 10^{-2}$	$4·33 \times 10^{-3}$
0·01	1·8	1·0	1·5	3·8	$6·48 \times 10^{-2}$	$2·86 \times 10^{-3}$
0·025	1·8	1·0	1·5	10·6	$1·11 \times 10^{-2}$	$1·32 \times 10^{-3}$
0·01	1·7	1·0	1·5	1·06	$4·66 \times 10^{-2}$	$7·54 \times 10^{-3}$
0·025	1·8	1·0	1·5	3·8	$6·39 \times 10^{-2}$	$6·44 \times 10^{-3}$
0·05	1·8	1·0	1·5	10·6	$1·19 \times 10^{-2}$	$2·56 \times 10^{-3}$
0·01	1·7	1·0	1·5	1·06	$4·66 \times 10^{-2}$	$7·54 \times 10^{-3}$
0·01	1·8	1·0	1·5	3·8	$6·26 \times 10^{-2}$	$1·11 \times 10^{-2}$
0·25	1·8	1·0	1·5	10·6	$1·83 \times 10^{-2}$	$1·04 \times 10^{-2}$
0·005	1·7	0·25	2·0	1·06	$1·01 \times 10^{-1}$	$4·65 \times 10^{-3}$
0·01	1·8	0·25	2·0	3·8	$5·34 \times 10^{-2}$	$2·13 \times 10^{-3}$
0·025	1·8	0·25	2·0	10·6	$4·78 \times 10^{-3}$	$9·27 \times 10^{-4}$
0·01	1·7	0·25	2·0	1·06	$1·00 \times 10^{-1}$	$8·33 \times 10^{-3}$
0·025	1·8	0·25	2·0	3·8	$5·11 \times 10^{-2}$	$5·00 \times 10^{-3}$
0·05	1·8	0·25	2·0	10·6	$5·60 \times 10^{-3}$	$1·83 \times 10^{-3}$
0·01	1·7	0·25	2·0	1·06	$1·00 \times 10^{-1}$	$8·33 \times 10^{-3}$
0·05	1·8	0·25	2·0	3·8	$5·14 \times 10^{-2}$	$9·06 \times 10^{-3}$
0·25	1·8	0·25	2·0	10·6	$1·18 \times 10^{-2}$	$8·36 \times 10^{-3}$

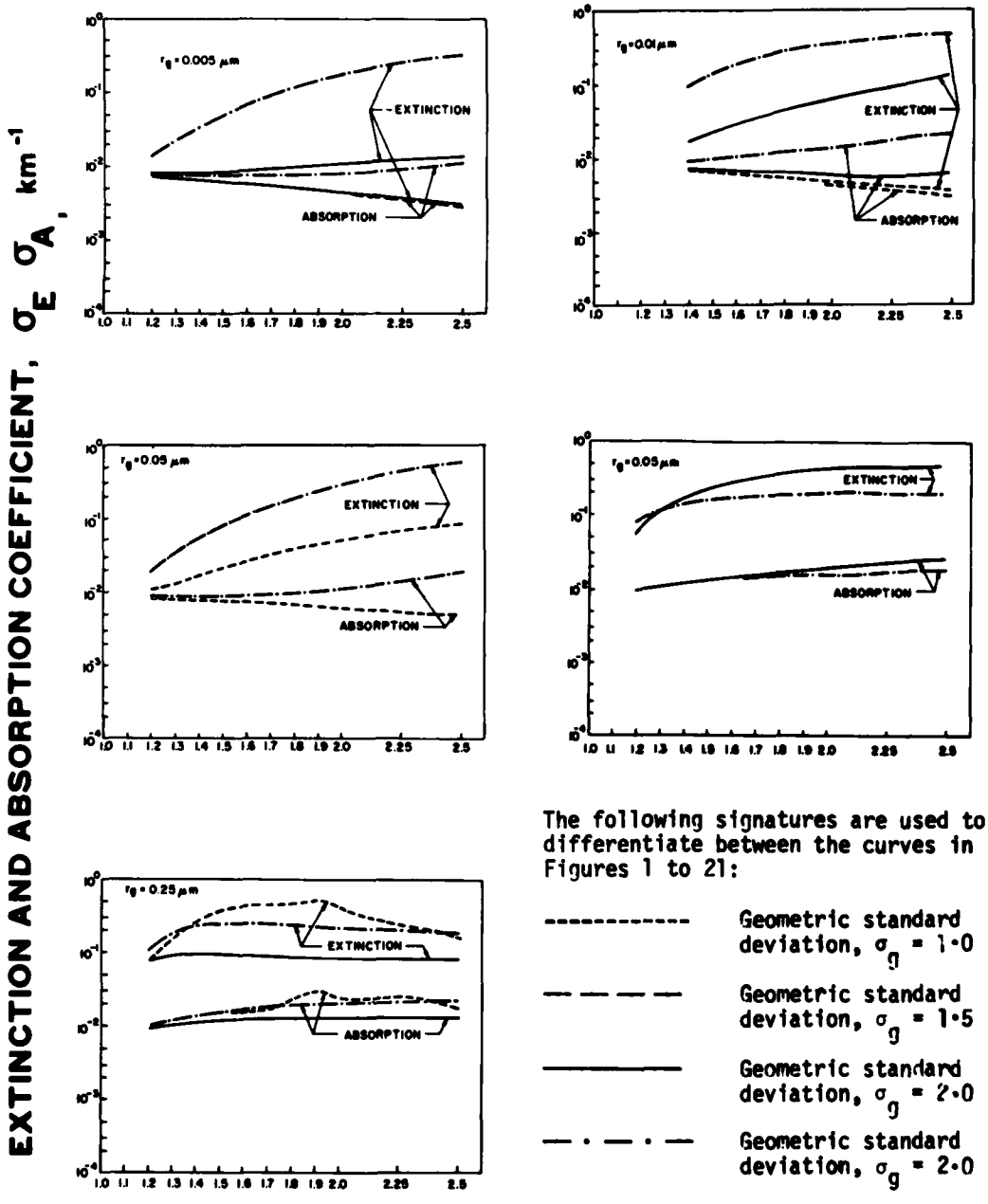

Figure 1. Volume extinction and absorption coefficients, σ_E and σ_A km^{-1} as a function of real index n. Wavelength λ = 0.55μm; imaginary index k = 0.01.

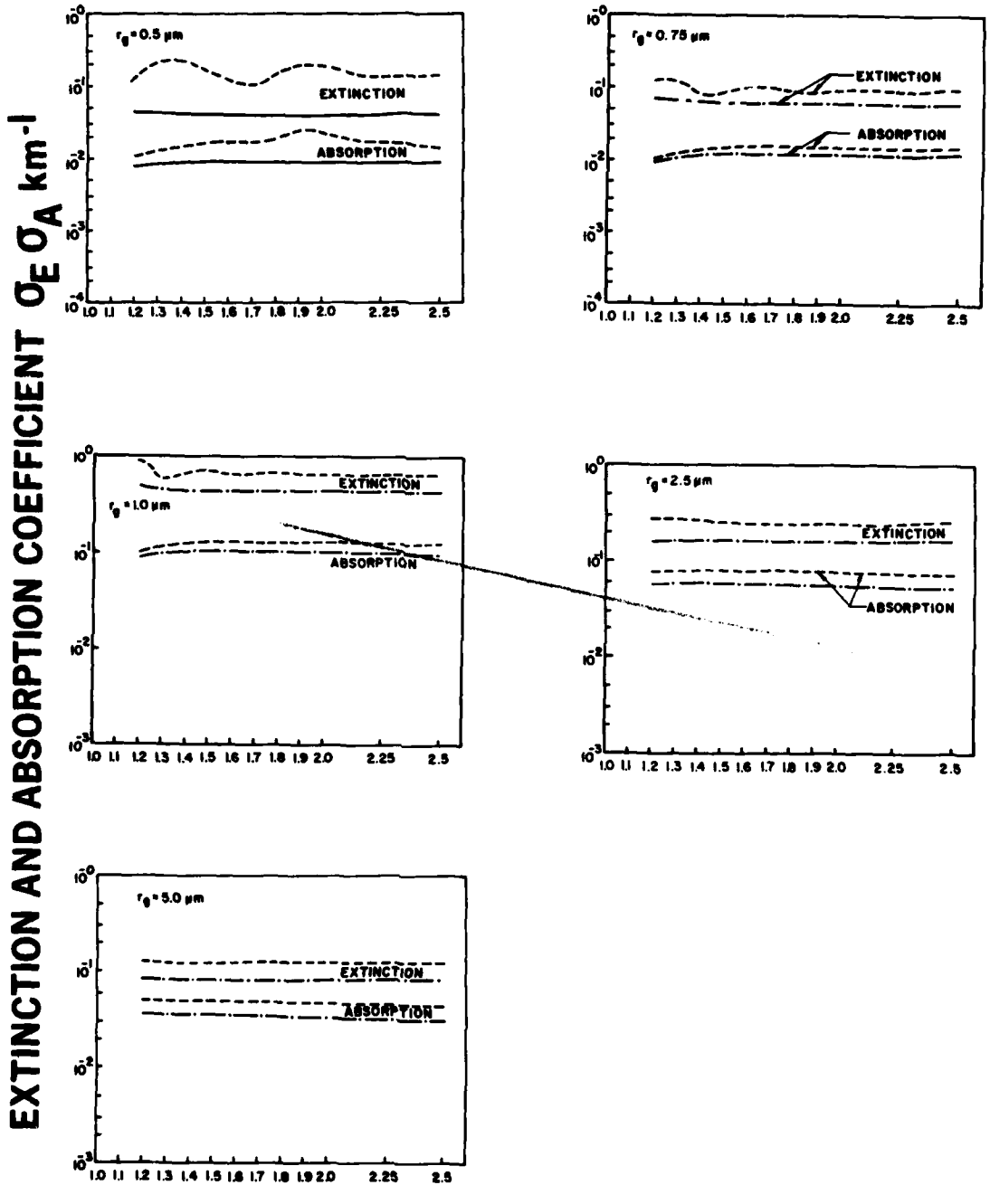

Figure 2. Volume extinction and absorption coefficients, σ_E and σ_A km^{-1} as a function of real index n. Wavelength λ = 0.55μm; imaginary index k = 0.01.

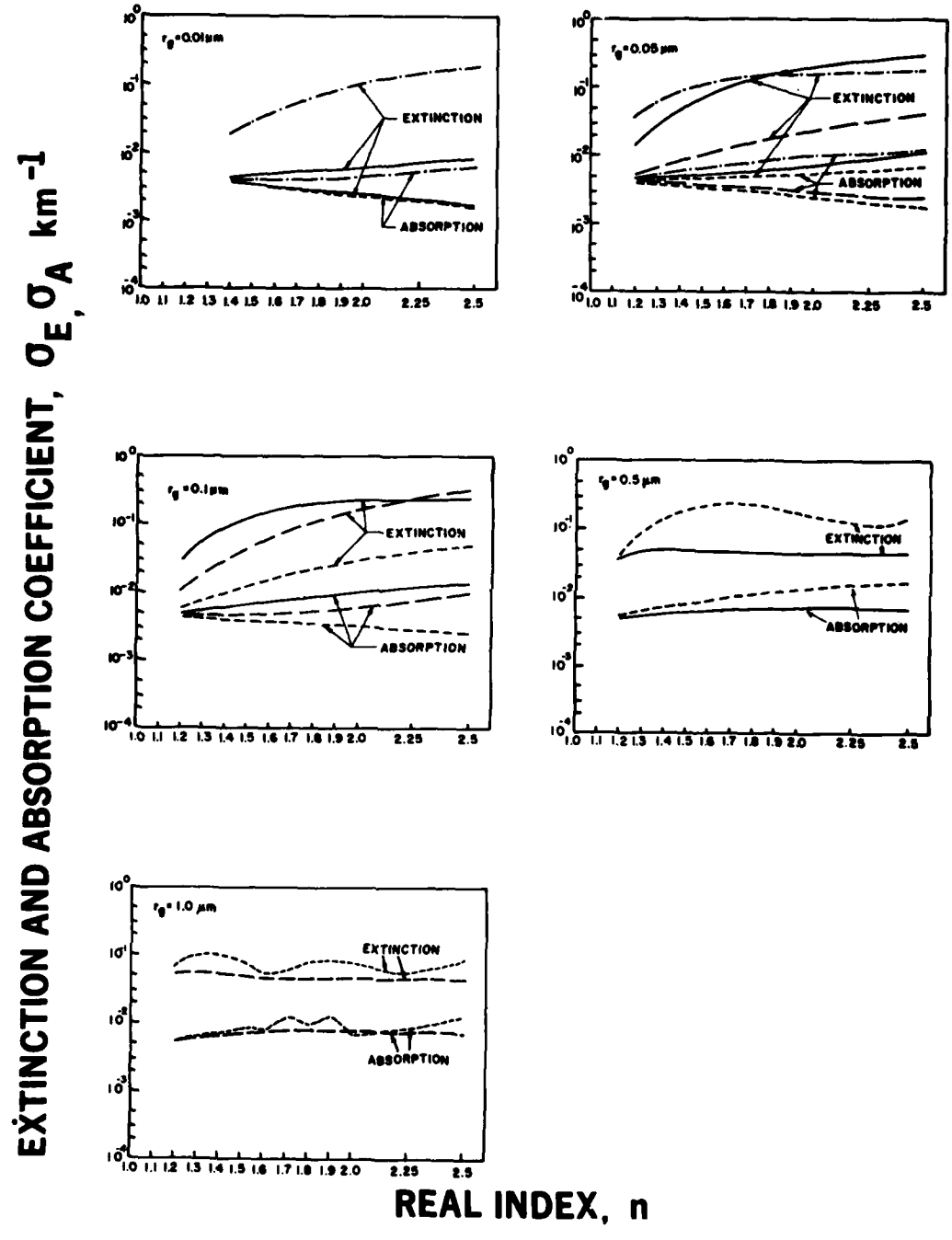

Figure 3. Volume extinction and absorption coefficients, σ_E and σ_A km^{-1} as a function of real index n. Wavelength λ = 1.06μm; imaginary index k = 0.01.

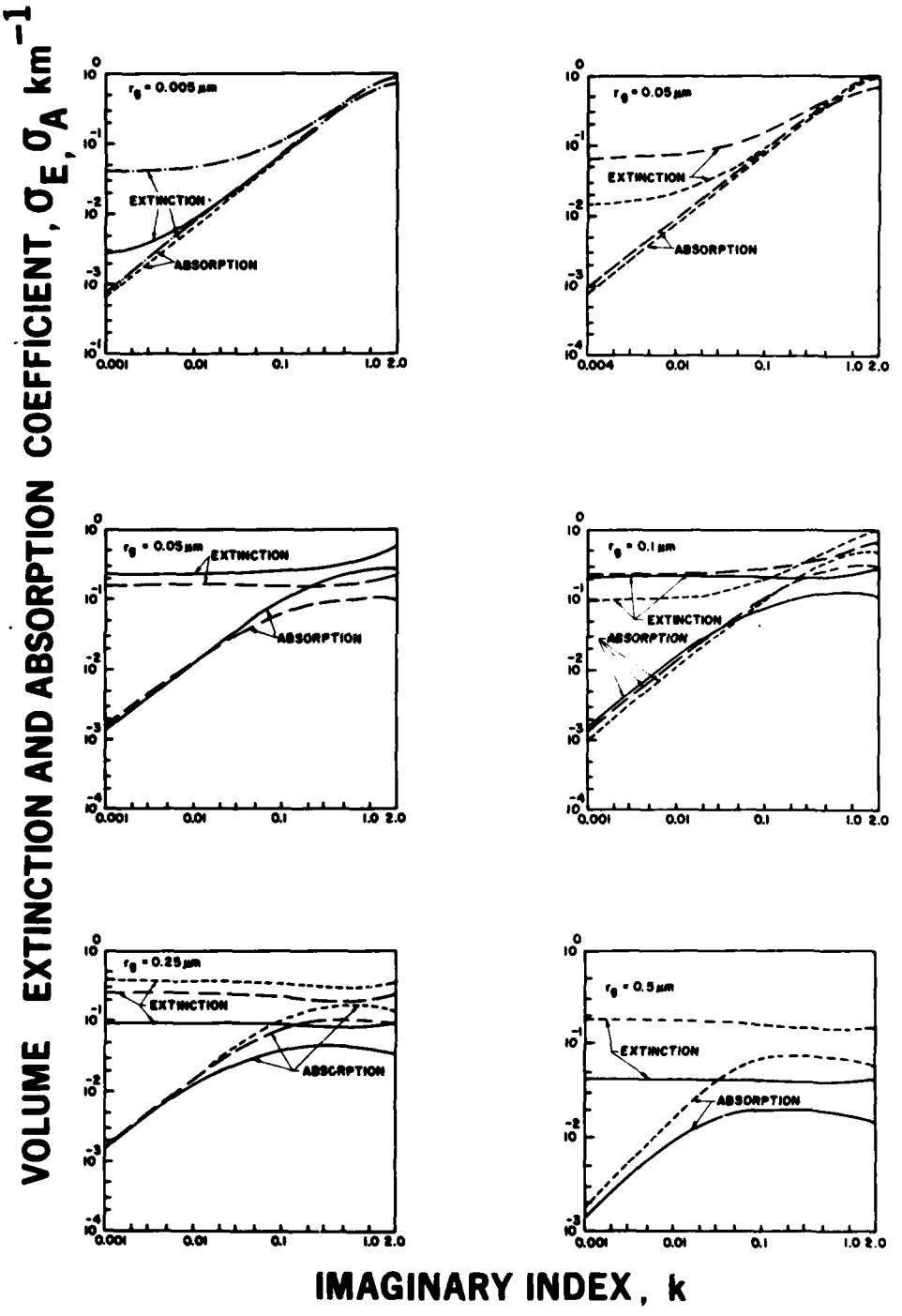

Figure 4. Volume extinction and absorption coefficients, km^{-1} as a function of imaginary index k. Wavelength λ = 0.55μm; real index n = 1.5.

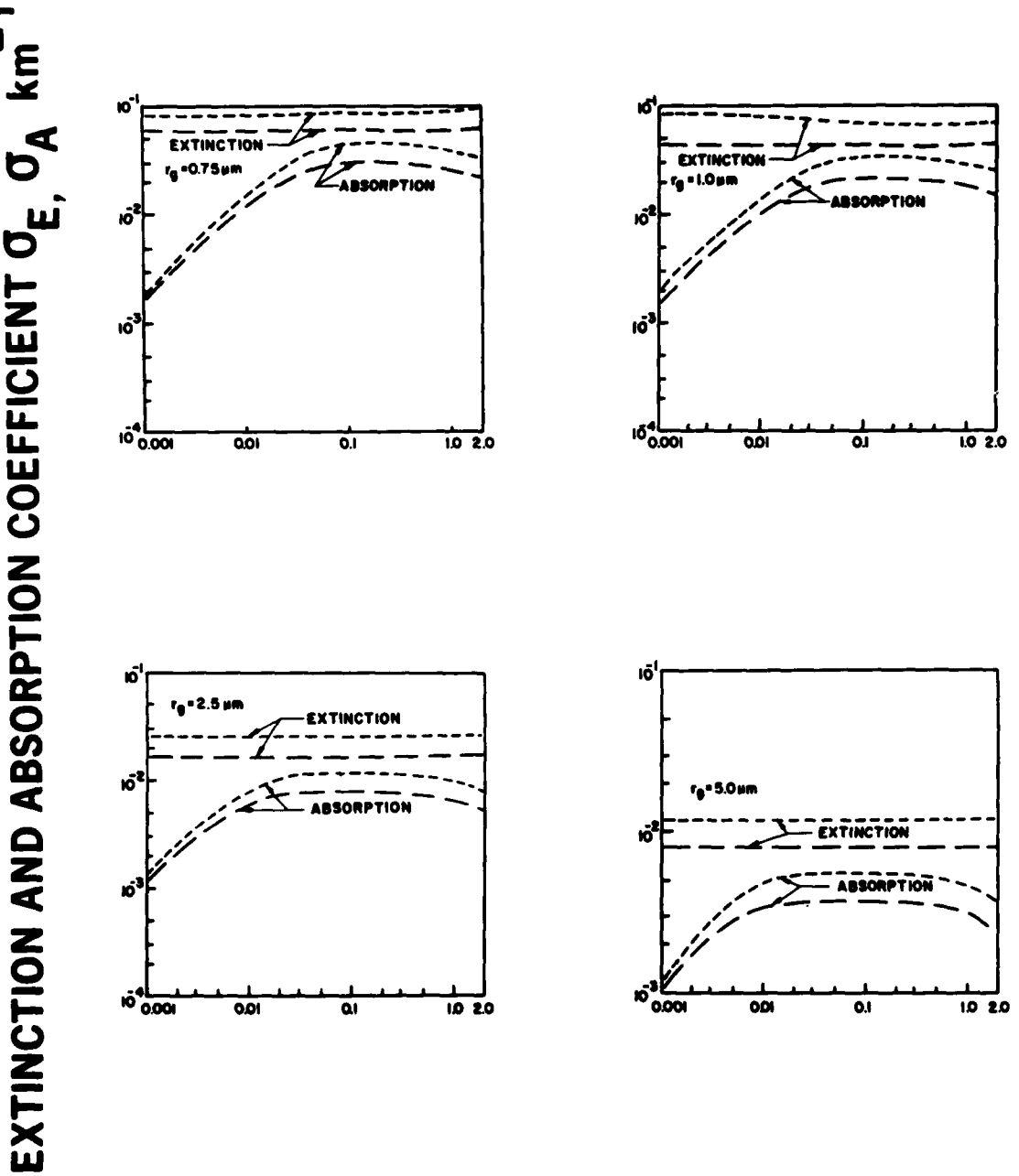

Figure 5. Volume extinction and absorption coefficients, km^{-1} as a function of imaginary index k. Wavelength λ = 0.55μm, real index = 1.5.

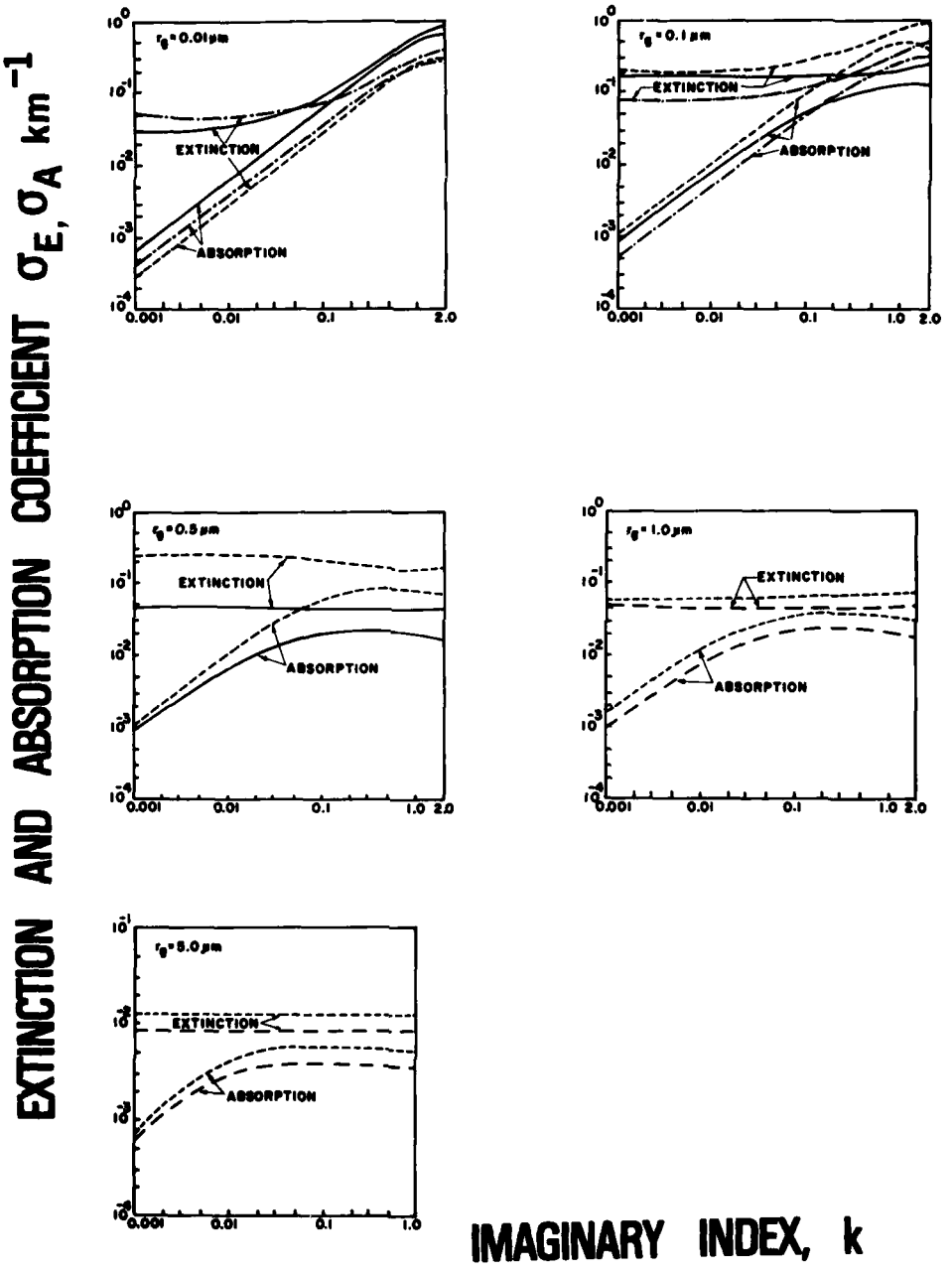

Figure 6. Volume extinction and absorption coefficients, σ_E and σ_A km^{-1} as a function of imaginary index k. Wavelength λ = 1.06μm; real index = 1.7.

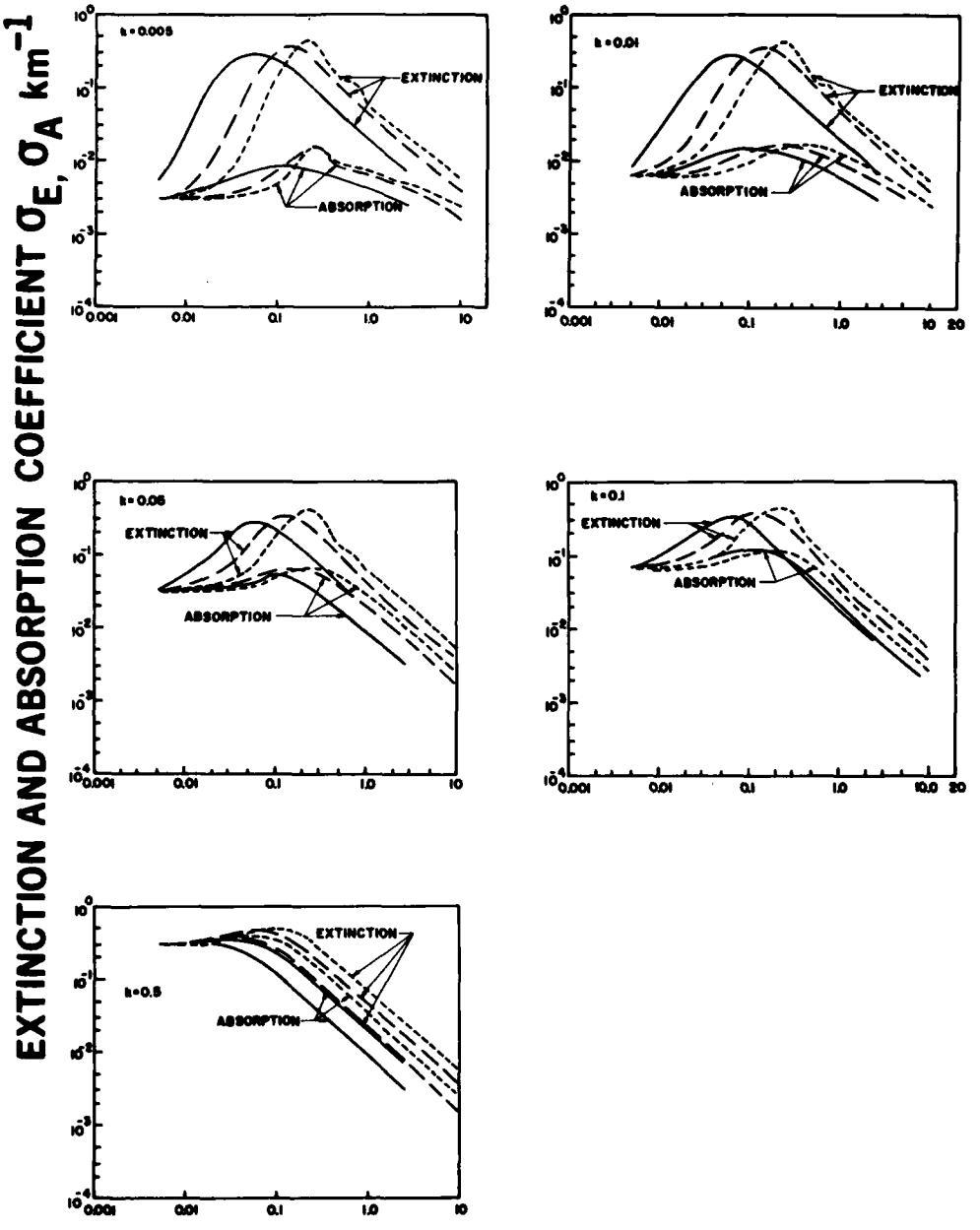

Figure 7. Extinction and absorption coefficient as a function of geometric mean radius r_g. Wavelength λ = 0.55μm; real index = 1.6.

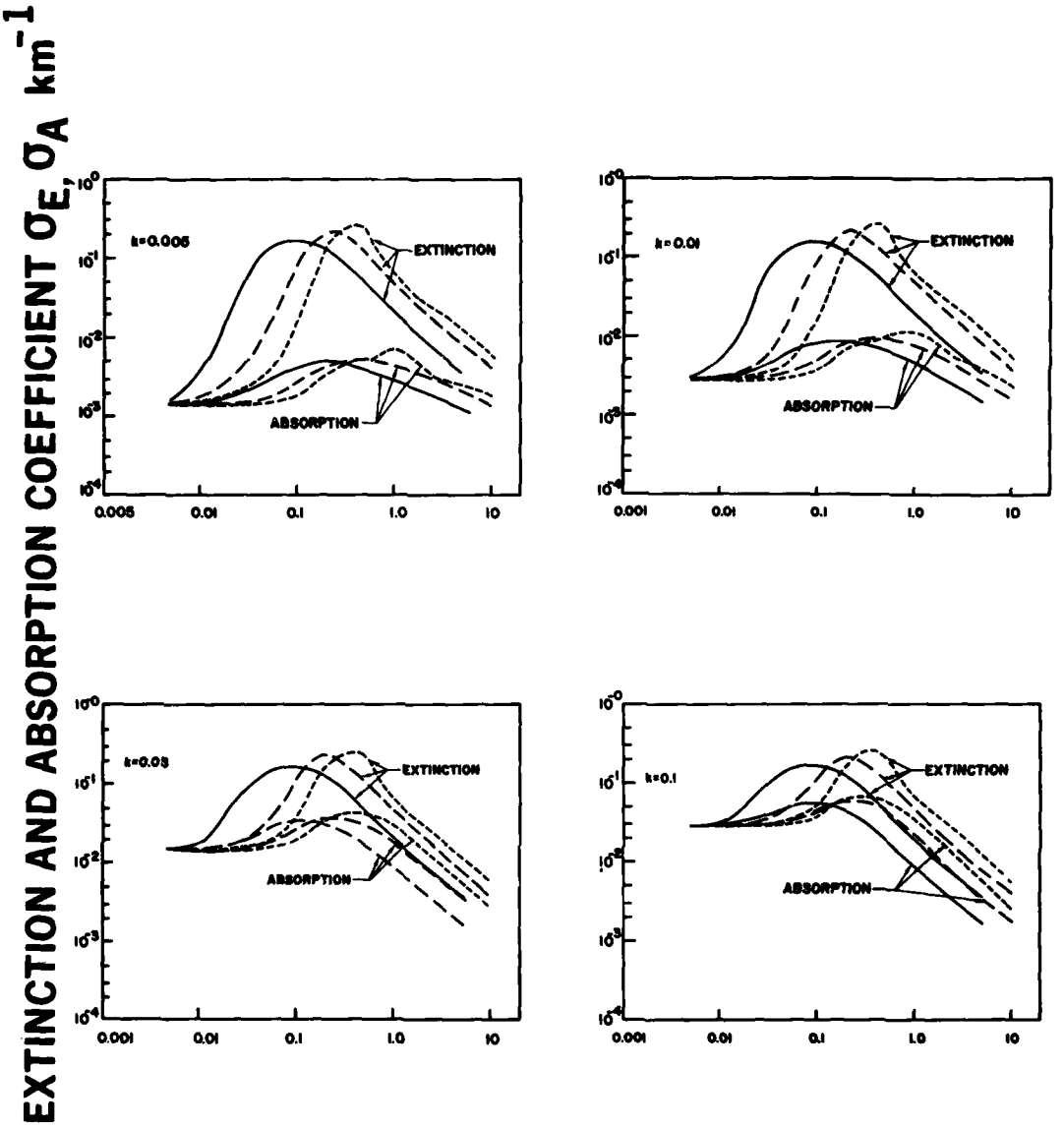

Figure 8. Volume extinction and absorption coefficient as a function of geometric mean radius r_g. Wavelength λ = 1.06μm; real index = 1.7.

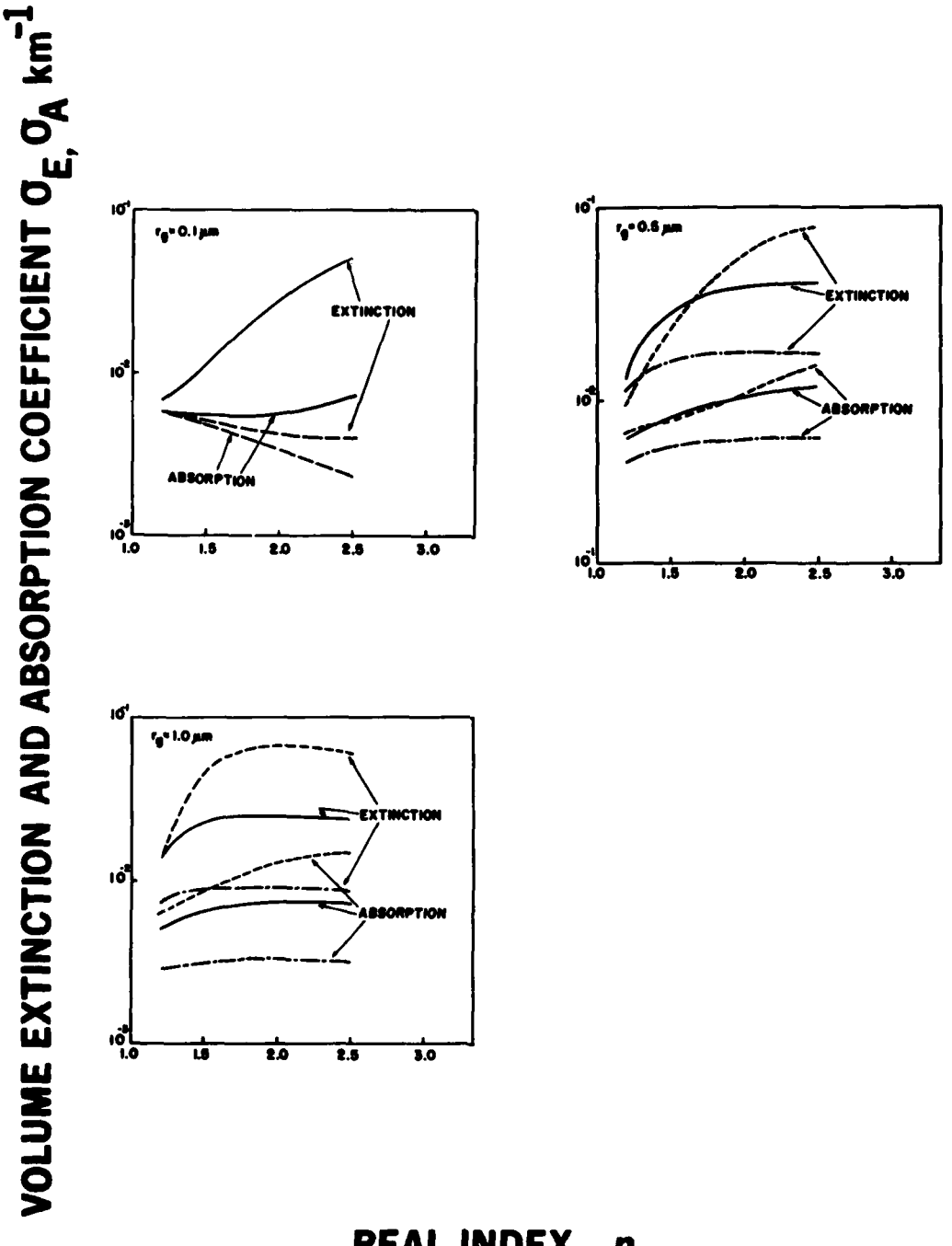

Figure 9. Volume extinction and absorption coefficient as a function of real index n. Wavelength λ = 3.8μm; imaginary index = 0.05.

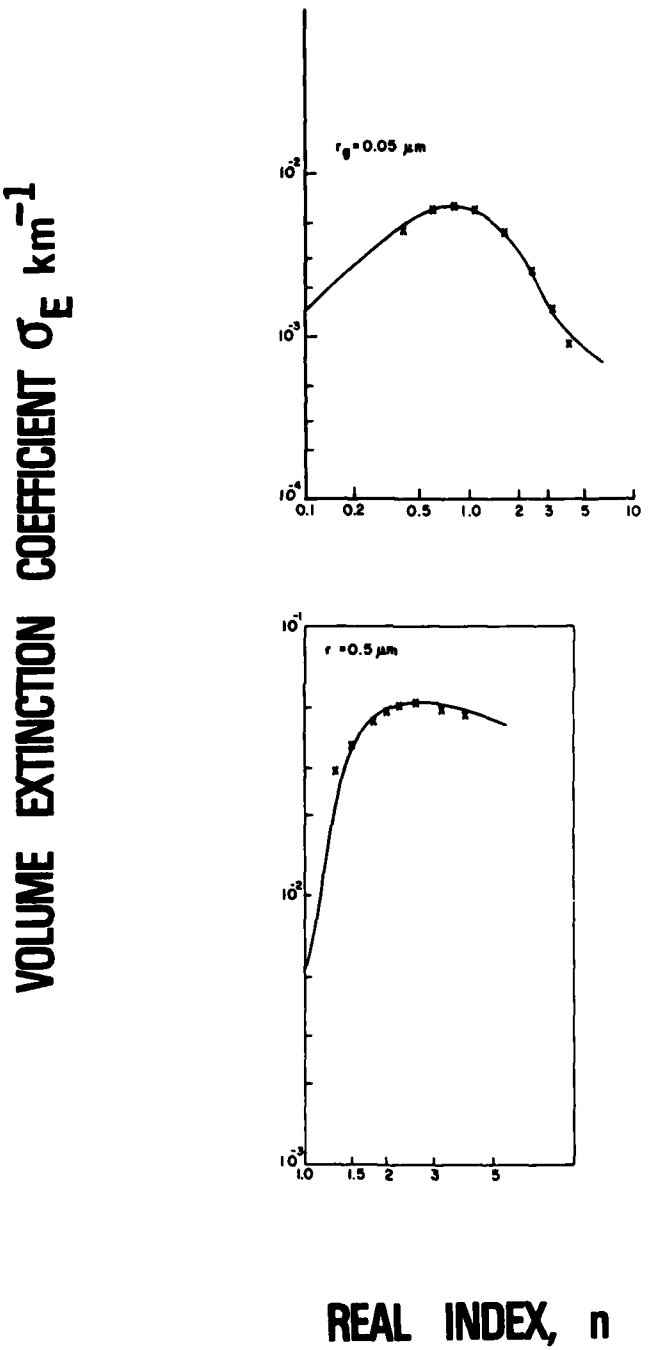

Figure 10. Volume extinction coefficient as a function of real index. Wavelength λ = 3.8μm; imaginary index k = 0.05. Points marked x satisfy Eq. (20). For upper curve n_g = 0.8, σ_n = 2.25; for lower curve σ_g = 2.0, n_g = 2.6, σ_n = 1.9.

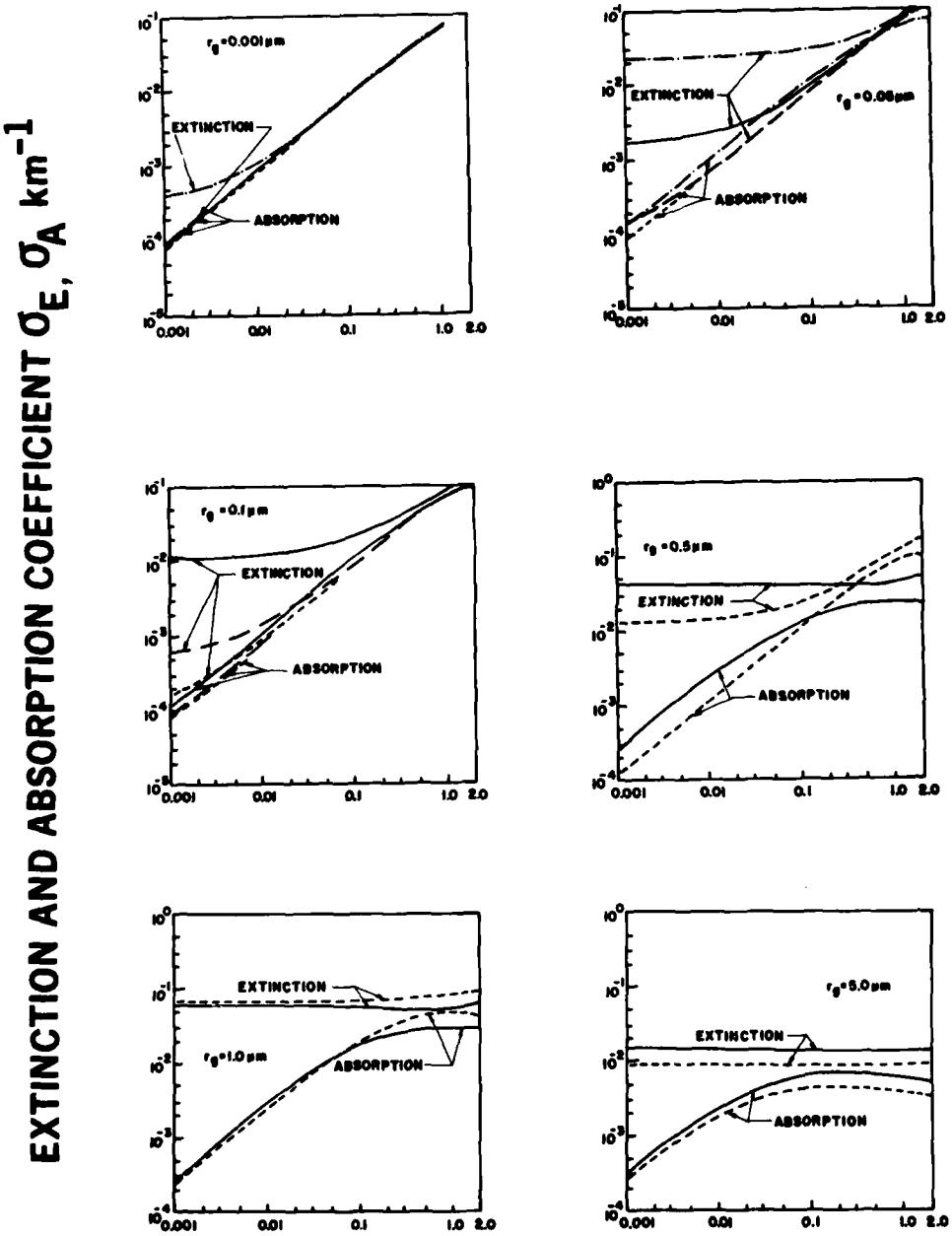

Figure 11. Volume extinction and absorption coefficient as a function of imaginary index k. Wavelength λ = 3.8μm; real index n = 1.7.

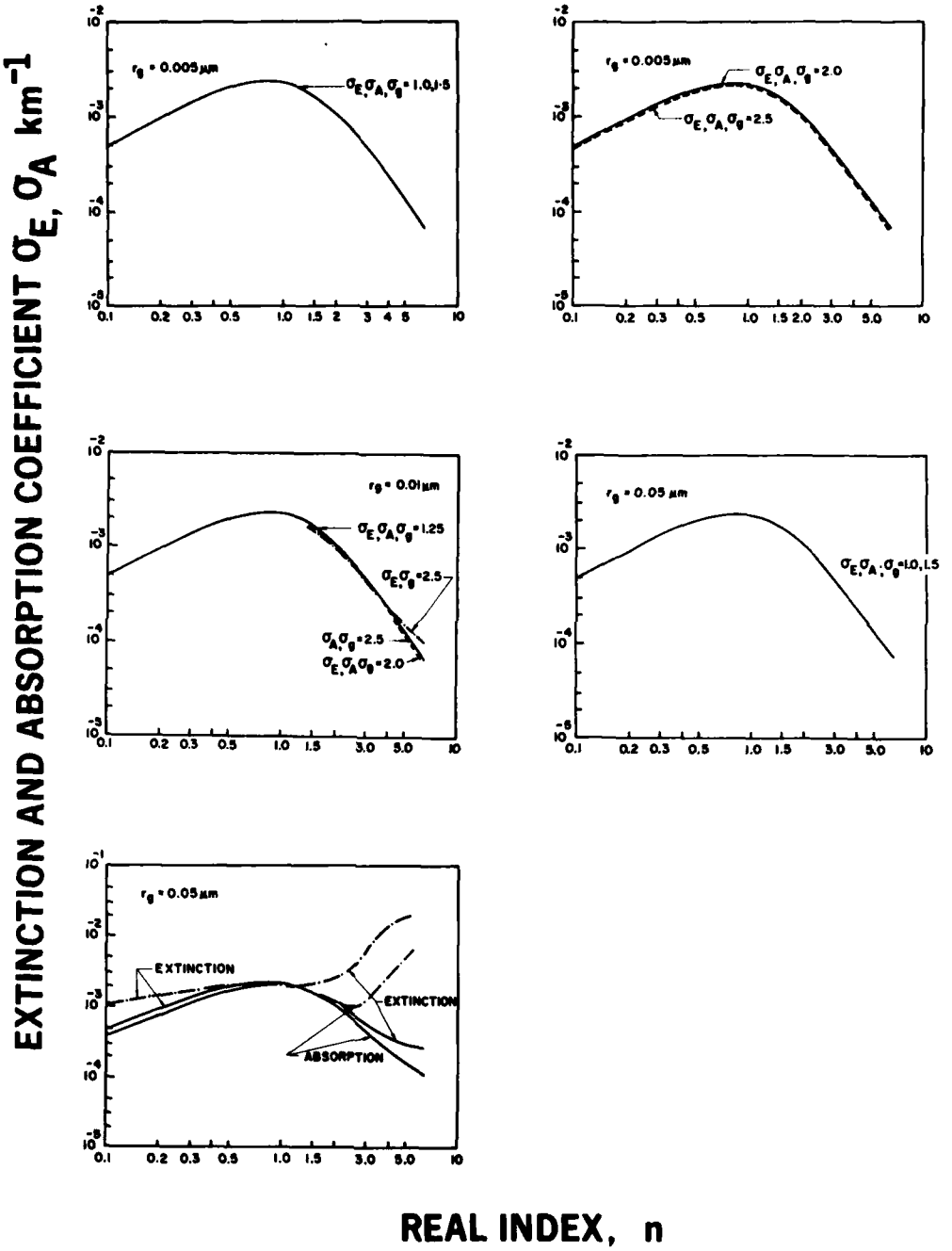

Figure 12. Volume extinction and absorption coefficient as a function of real index. Wavelength λ = 10.6μm; imaginary index k = 0.05.

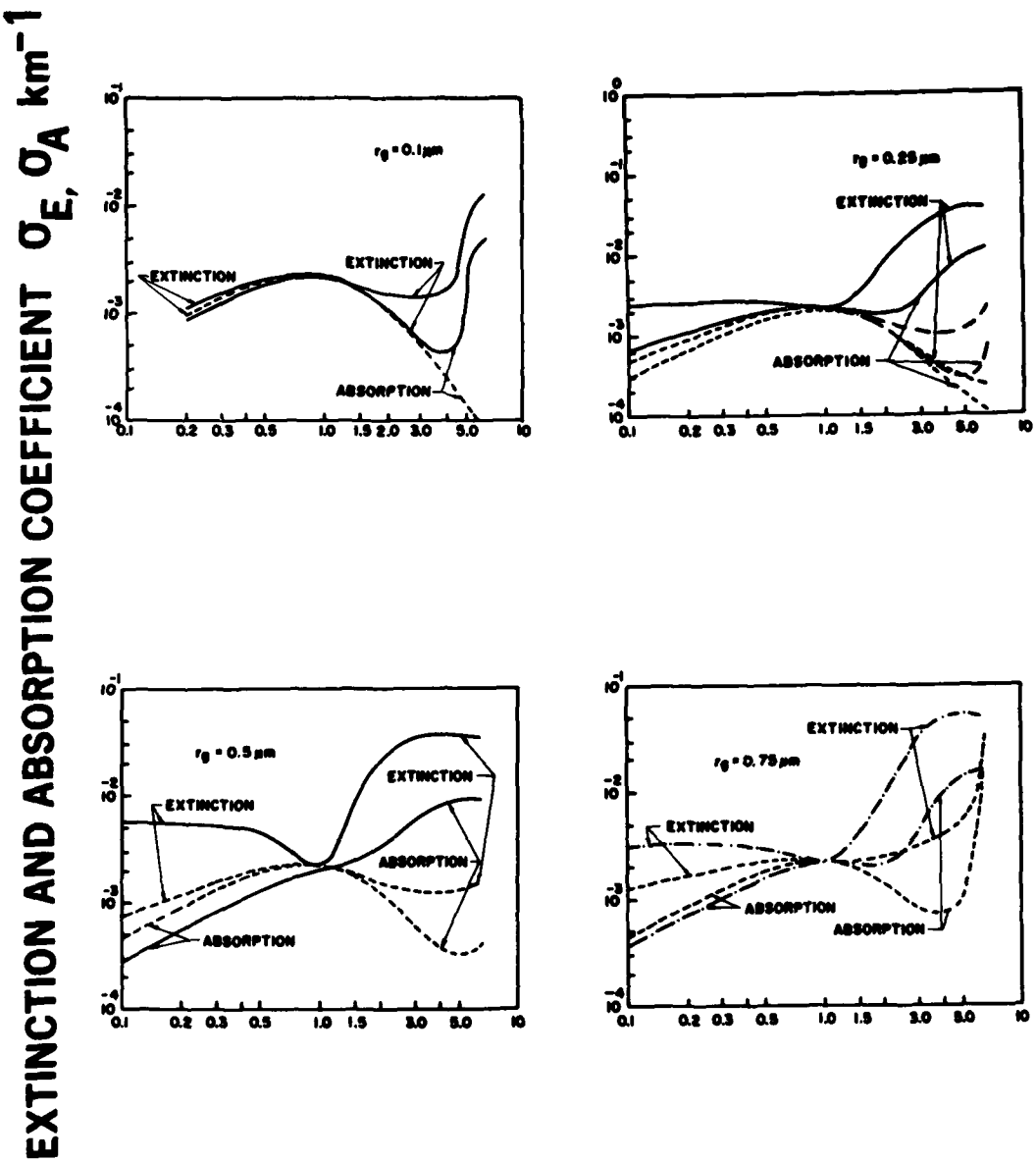

Figure 13. Volume extinction and absorption coefficient as a function of real index. Wavelength λ = 10.6μm; imaginary index = 0.05.

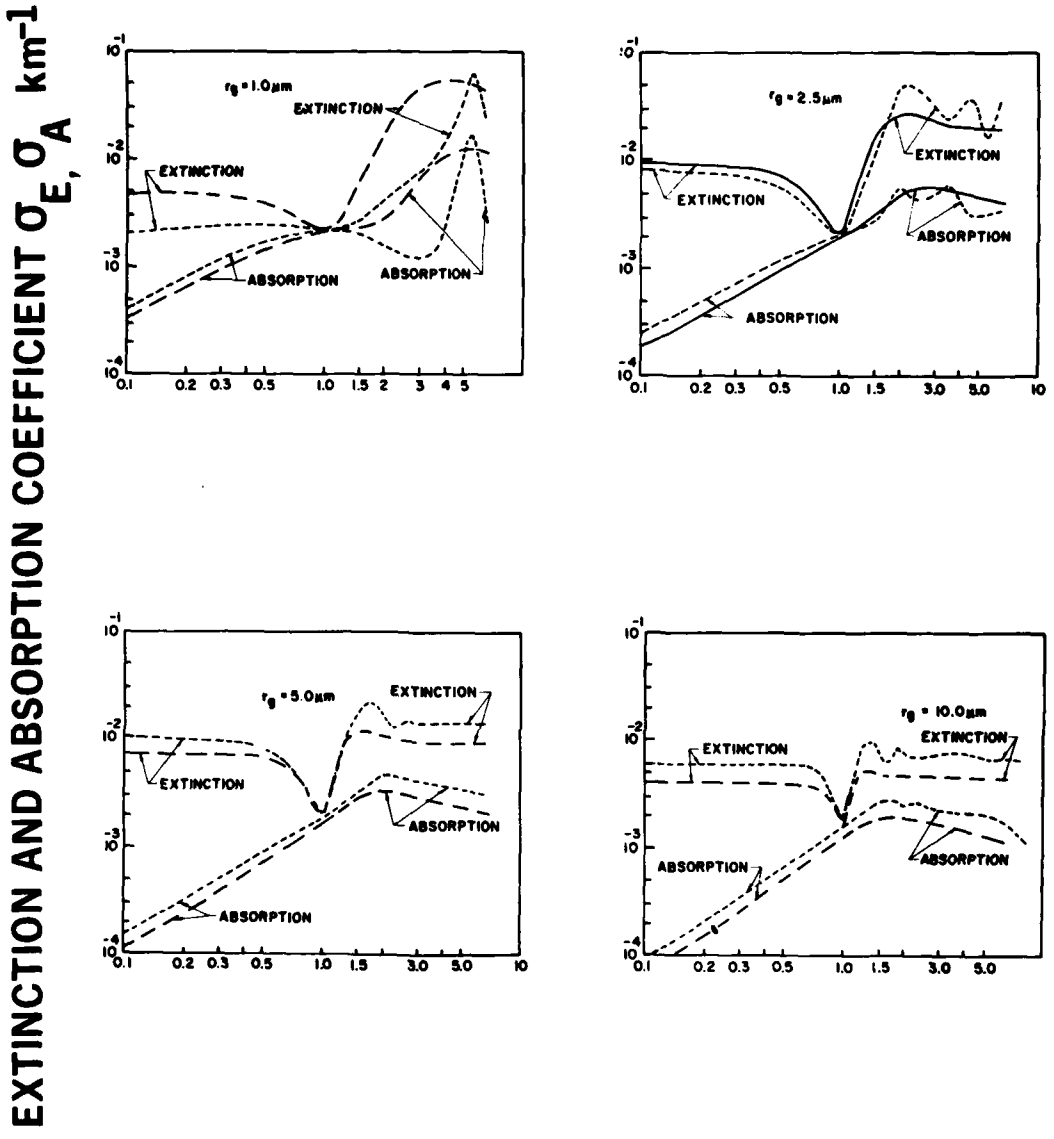

Figure 14. Volume extinction and absorption coefficient as a function of real index. Wavelength λ = 10.6μm; imaginary index k = 0.05.

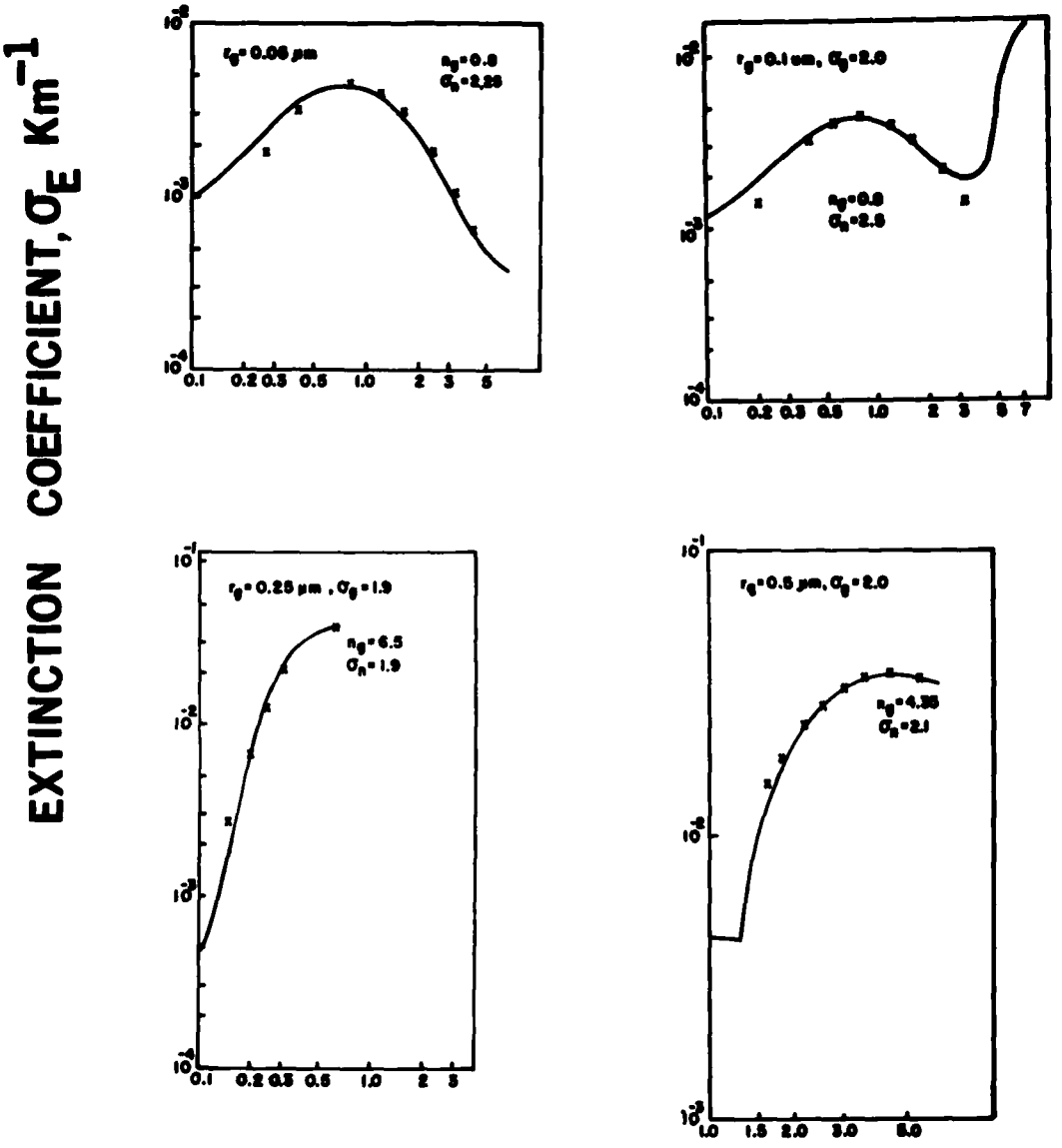

Figure 15. Volume extinction coefficient as a function of real index. Wavelength λ = 10.6μm; imaginary index k = 0.1. Points marked x satisfy Eq. (20).

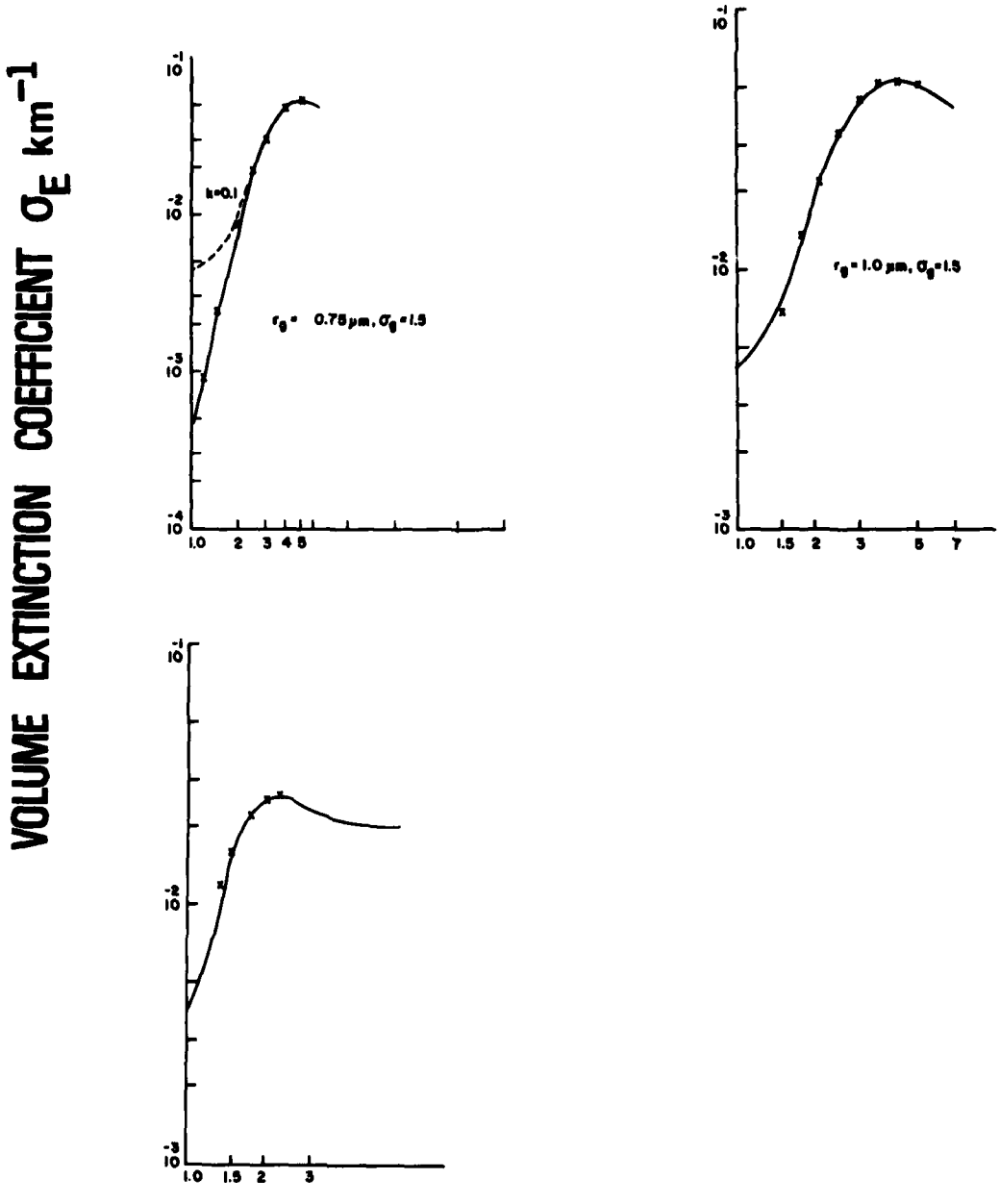

Figure 16. Volume extinction coefficient as a function of real index. Wavelength = 10.6μm; imaginary index = 0.1. Points marked x satisfy Eq. (20).
Top left curve: $n_g = 5.0$, $\sigma_n = 1.625$ for $k = 0.01$, $\sigma_n = 1.65$ for $k = 0.1$ (dashed curve).
Top right curve: $n_g = 4.2$, $\sigma_n = 1.65$
Bottom curve: $r_g = 2.5\mu m$, $\sigma_g = 1.5$; $n_g = 2.25$, $\sigma_n = 1.5$

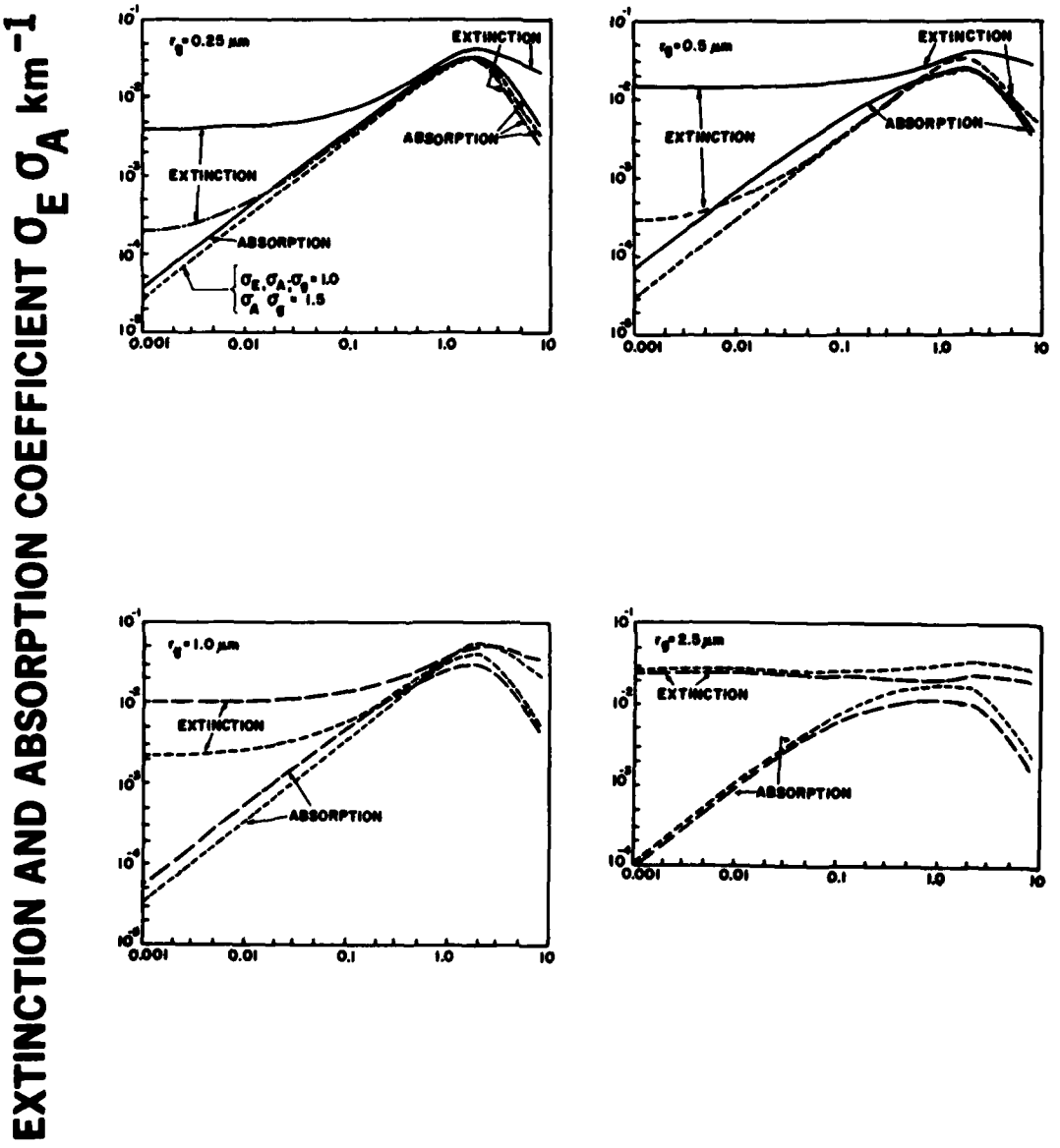

Figure 17. Volume extinction and absorption coefficient as a function of imaginary index. Wavelength = 10.6μm; real index = 1.8.

VOLUME EXTINCTION AND ABSORPTION COEFFICIENT σ_E σ_A km^{-1}

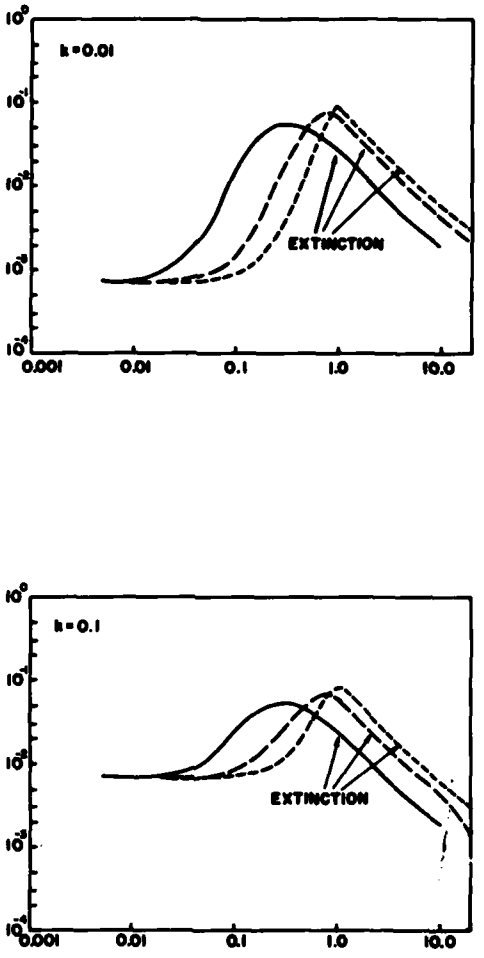

GEOMETRIC MEAN RADIUS, rg (um)

Figure 18. Volume extinction coefficient as a function of geometric mean radius. Wavelength = 3.8μm; real index = 1.8.

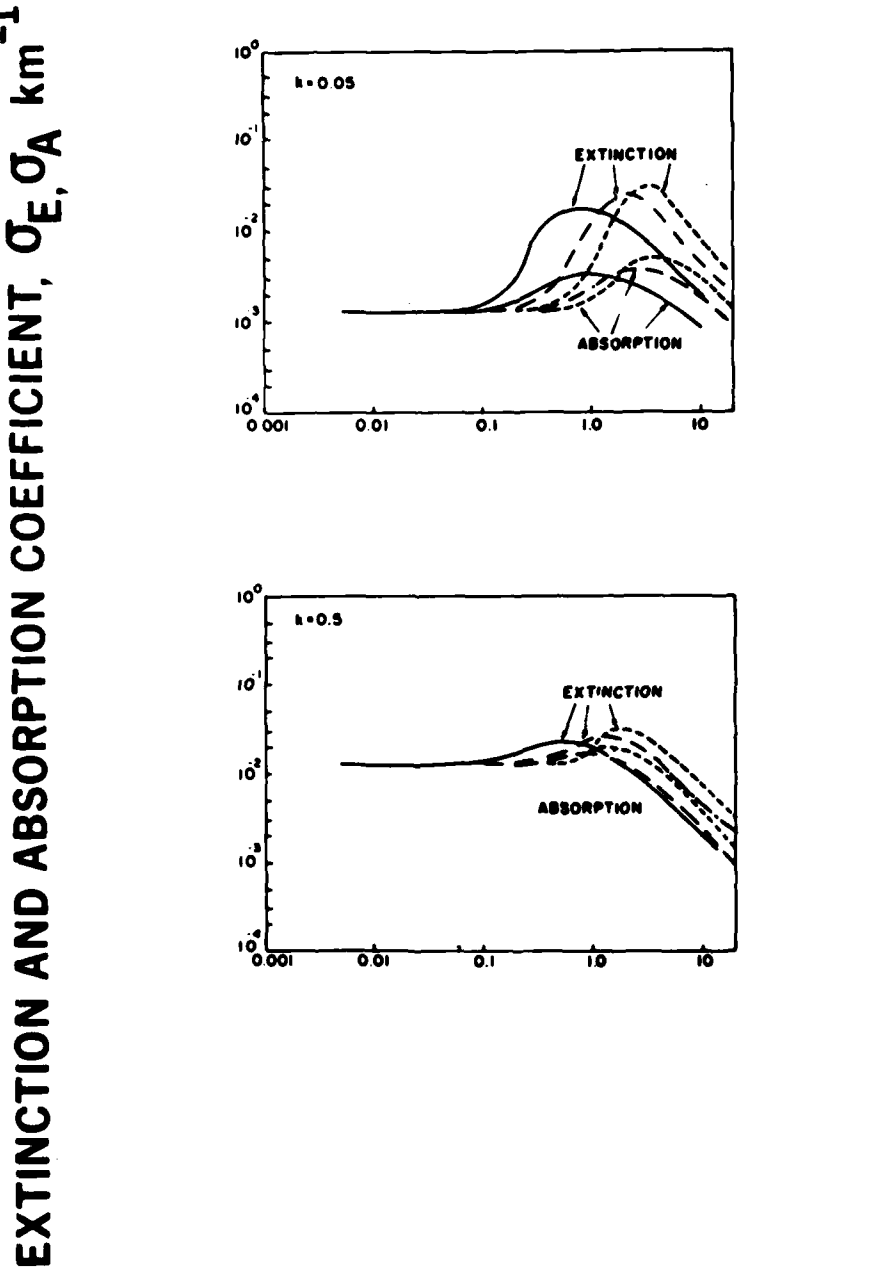

Figure 19. Volume extinction and absorption coefficient as a function of geometric mean radius. Wavelength = 10.6μm; real index = 1.8.

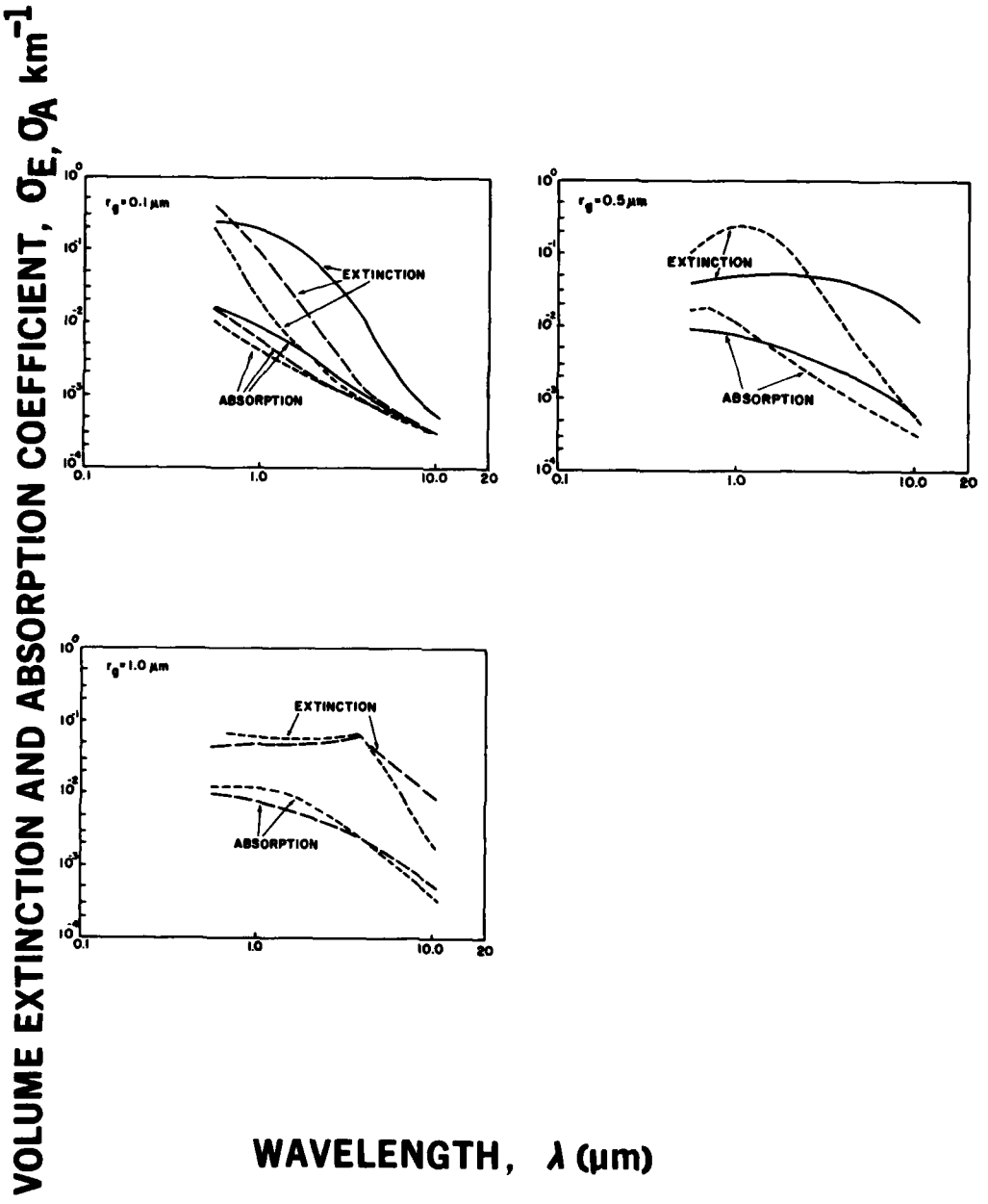

Figure 20. The variation of extinction and absorption coefficient with wavelength. Real index = 1.7, imaginary index = 0.01.

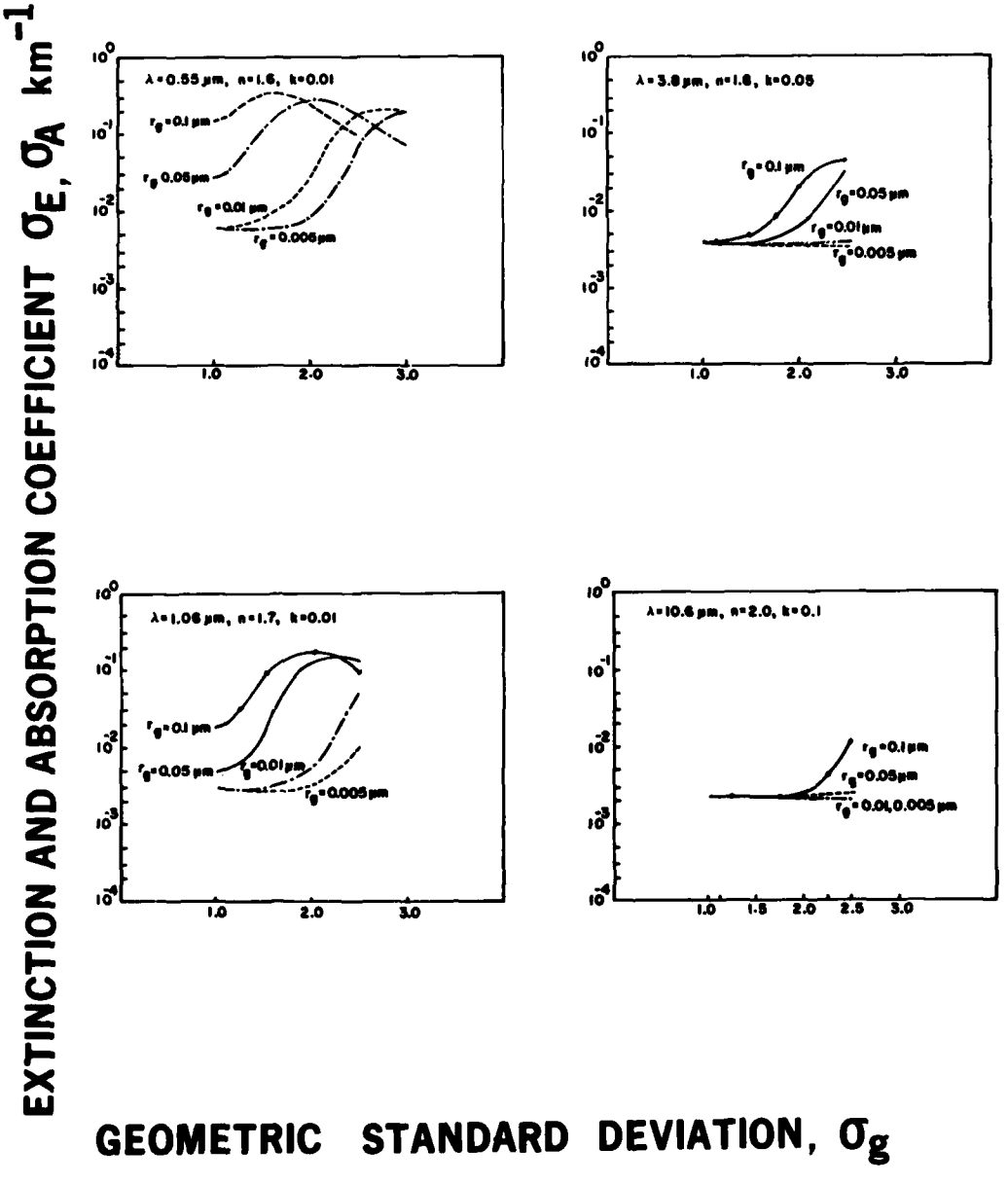

Figure 21. The variation of volume extinction coefficient with geometric standard deviation.

REFERENCES

1. Mie, G., 1908, "Beitraeg Zur Optik Trueber Medien," Ann. Physik., 25:377-445.

2. van de Hulst, H. C., 1957, Light Scattering by Small Particles, New York, Wiley.

3. Deirmendjian, D., 1969, Electromagnetic Scattering on Spherical Polydispersions, New York, Elsevier.

4. Kerker, M., 1969, The Scattering of Light and Other Electromagnetic Radiation, New York, Academic Press.

5. Blättner, W. G. M., 1977, Research Note RRA-N-7703, Radiation Research Associates.

6. Grams, G. W., 1978, private communication.

7. Patterson, E. M., and D. A. Gillette, 1977, "Commonalities in Measured Size Distributions for Aerosols having a Soil-Derived Component," J. Geophys. Res., 82:2074-2082.

8. Whitby, K. T., W. E. Clark, V. A. Marple, G. M. Sverdrup, G. J. Sem, K. Willeke, B. Y. H. Liu, and D. Y. H. Pui, 1975, "Characterization of California Aerosols - I: Size Distributions of Freeway Aerosols," Atmospheric Environment, 9:463-482.

9. Davies, C. N., 1974, "Size Distributions of Atmospheric Particles," Aerosol Science, 5:293-300.

10. Hanel, G., 1968, "The Real Part of the Mean Complex Refractive Index and the Mean Density of Samples of Atmospheric Aerosol Particles," Tellus, 20:371-379.

11. Chylek, Peter, 1973, "Large-Sphere Limits of Mie-Scattering Functions," J. Opt. Soc. Am., 63:699-706.

12. Toon, O. B., J. B. Pollack, and B. N. Khare, 1976, "Optical Constants of Several Atmospheric Aerosol Species, Ammonium Sulphate, Aluminum Oxide and Sodium Chloride," J. Geophys. Res., 81:5733-5748.

13. Downing, H. D., L. W. Pinkley, P. P. Sethna, and D. Williams, 1974, "Optical Constants of Ammonium Sulphate in the Infrared," J. Opt. Soc. Am., 67:186-190.

14. Querry, M. R., W. E. Holland, and R. C. Waring, 1976, "Complex Refractive Index in the Infrared for NaCl, Na NO_3 and Na HCO_3 in Water," J. Opt. Soc. Am., 66:830-836.

15. Hale, G. M., and M. R. Querry, 1973, "Optical Constants of Water in the 200-nm to 200-μm Wavelength Region," Applied Optics, 12:555-563.

16. Spitzer, W. G., and D. A. Kleinman, 1961, "Infrared Lattice Bands of Quartz," Phys. Rev., 121:1324.

17. Peterson, J. T., and J. A. Weinman, 1969, "Optical Properties of Quartz Dust Particles at Infrared Wavelengths," J. Geophys. Res., 74:6947-6952.

18. Palmer, K. F., and D. Williams, 1975, "Optical Constants of Sulphuric Acid; Application to the Clouds of Venus," Applied Optics, 14:208-219.

19. Foster, P. J. and C. R. Howarth, 1968, "Optical Constants of Carbons and Coals in the Infrared," Carbon, 6, pp. 719-729.

20. McCartney, J. T., J. B. Yasinsky, and S. Ergun, 1965, "Optical Constants of Coals," Fuel, 44, pp. 349-354.

21. Twitty, J. T. and J. A. Weinman, 1971, "Radiative Properties of Carbonaceons Aerosols," J. Appl. Meteorol., 10:725-731.

22. Dalzell, W. H. and A. F. Sarofim, 1969, "Optical Constants of Soot and their Application to Heat Flux Calculations," J. Heat Transfer 91:100-104.

23. Tyler, I. L., and M. R. Querry, 1977, "Complex Refractive Index in the Infrared for $ZnC\ell_2$ in Water," Phys. Rev.

24. Querry, M. R., G. Osborne, K. Lies, R. Jurdan, and R. M. Coveney, 1977, "Complex Refractive Index of Limestone in the Visible and Infrared," Applied Optics.

25. Toon, O. B., J. B. Pollack, and C. Sagan, 1977, "Physical Properties of the Particles Composing the Martian Dust Storm of 1971-1972," Icarus, 30:663-696.

26. Fischer, K., 1973, "Mass Absorption Coefficient of Natural Aerosol Particles in the 0.4μm-2.4μm Wavelength Interval," Beit. Phys. Atmos., 46:89-100.

27. Fischer, K., 1975, "Mass Absorption Indices of Various Types of Natural Aerosol Particles in the Infrared," Applied Optics, 14:2851-2856.

28. Lindberg, J. D., and L. S. Laude, 1974, "Measurement of the Absorption Coefficient of Atmospheric Dust," Applied Optics, 13:1923-1927.

29. Herman, B. M., R. S. Browning, J. J. DeLuisi, 1975, "Determination of the Effective Imaginary Term of the Complex Index of Atmospheric Dust by Remote Sensing: The Diffuse-Direct Radiation Method," J. Atmospheric Sci., 32:918-925.

30. Grams, G. W., I. H. Blifford, D. A. Gillette, and P. B. Russel, 1974, "Complex Index of Refraction of Airborne Soil Particles," J. Appl. Meteorol., 13:459-471.

31. Patterson, E. M., D. A. Gillette, and B. H. Sfocklin, 1977, "Complex Index of Refraction between 300 and 700 nm for Saharan Aerosols," Applied Optics (in press).

32. Hoidale, G. B., and A. J. Blanco, 1969, "Infrared Absorption Spectro of Atmospheric Dust over an Interior Desert Basin," Pure and Applied Geophys., 74:151-164.

33. Sverdrup, G. M., K. T. Whitby, and W. E. Clark, 1975, "Characterization of California Aerosols - II: Aerosol Size Distribution Measurements in the Mojave Desert," Atmospheric Environment, 9:483-494.

34. Hoihjelle, D. L., R. G. Pinnick, J. D. Lindberg, R. B. Loveland, E. B. Stenmark, C. J. Petracca, 1976, "Balloon-Borne Aerosol Particle Counter Measurements Made in Wintertime at Grafenwöhr, West Germany," ECOM-DR-76-3, Atmospheric Sciences Laboratory, US Army Electronics Command, White Sands Missile Range, NM.

35. De Luisi, J. J., P. M. Furukana, D. A. Gillette, B. G. Schuster, R. T. Charlson, W. M. Porch, R. W. Fegley, B. M. Herman, R. A. Rabinoff, J. T. Twitty, and J. A. Weinman, 1976, "Results of a Comprehensive Atmospheric Aerosol-Radiation Experiment in the Southwestern United States, Part I: Size Distribution, Extinction Optical Depth and Vertical Profiles of Aerosols Suspended in the Atmosphere," J Appl. Meteorol., 15:441-454.

36. Meszaros, A., and K. Vissy, 1974, "Concentration, Size Distribution and Chemical Nature of Atmospheric Aerosol Particle in Remote Oceanic Areas," Aerosol Science, 5:101-109.

37. Jennings, S. G., 1977, "Mie Theory Sensitivity Studies - The Effects of Aerosol Complex Refractive Index and Size Distribution Variations on Extinction and Absorption Coefficients Part I: Tabulated Computational Results, ECOM Data Report ECOM-DR-77-5, Atmospheric Sciences Laboratory, US Army Electronics Command, White Sands Missile Range, NM. AD A049031

38. Patterson, E. M., D. A. Gillette, and G. W. Grams, 1976, "The Relation between Visibility and the Size-Number Distribution of Airborne Soil Particles," J. Appl. Meteorol., 15:470-478.

39. Bergstron, R. W., 1973, "Extinction and Absorption Coefficients of the Atmospheric Aerosol as a Function of Particle Size," Beit. Phys. Atmos., 46:223-234.

40. Waggoner, A. P., M. B. Baker, and R. J. Charlson, 1973, "Optical Absorption by Atmospheric Aerosols," Applied Optics, 12:896.

41. Jennings, S. G., 1977, "The Absorption Coefficient as a Function of Complex Index of Refraction and Particle Size Distribution," ECOM report in preparation.

42. Plass, G. N., 1966, "Mie Scattering and Absorption Cross Sections for Absorbing Particles," Applied Optics, 5:279-285.

43. Schleusener, S. A., J. D. Lindberg, K. O. White, R. L. Johnson, 1976, "Spectrophone Measurements of Infrared Laser Energy Absorption by Atmospheric Dust," Applied Optics, 15:2546-2550.

44. Gradshteyn, I. S., and I. M. Ryzhik, 1965, Table of Integrals, Series, and Products, Academic Press, New York and London, p. 307.

DISTRIBUTION LIST

Director
US Army Ballistic Research Laboratory
ATTN: DRDAR-BLB, Dr. G. E. Keller
Aberdeen Proving Ground, MD 21005

Air Force Weapons Laboratory
ATTN: Technical Library (SUL)
Kirtland AFB, NM 87117

Commander
Headquarters, Fort Huachuca
ATTN: Tech Ref Div
Fort Huachuca, AZ 85613

6585 TG/WE
Holloman AFB, NM 88330

Commandant
US Army Field Artillery School
ATTN: Morris Swett Tech Library
Fort Sill, OK 73503

Commandant
USAFAS
ATTN: ATSF-CD-MT (Mr. Farmer)
Fort Sill, OK 73503

Director
US Army Engr Waterways Exper Sta
ATTN: Library Branch
Vicksburg, MS 39180

Commander
US Army Electronics Command
ATTN: DRSEL-CT-S (Dr. Swingle)
Fort Monmouth, NJ 07703
03

CPT Hugh Albers, Exec Sec
Interdept Committee on Atmos Sci
Fed Council for Sci & Tech
National Sci Foundation
Washington, DC 20550

Inge Dirmhirn, Professor
Utah State University, UMC 48
Logan, UT 84322

HQDA (DAEN-RDM/Dr. De Percin)
Forrestal Bldg
Washington, DC 20314

Commander
US Army Aviation Center
ATTN: ATZQ-D-MA
Fort Rucker, AL 36362

CO, USA Foreign Sci & Tech Center
ATTN: DRXST-ISI
220 7th Street, NE
Charlottesville, VA 22901

Director
USAE Waterways Experiment Station
ATTN: Library
PO Box 631
Vicksburg, MS 39180

US Army Research Office
ATTN: DRXRO-IP
PO Box 12211
Research Triangle Park, NC 27709

Mr. William A. Main
USDA Forest Service
1407 S. Harrison Road
East Lansing, MI 48823

Library-R-51-Tech Reports
Environmental Research Labs
NOAA
Boulder, CO 80302

Commander
US Army Dugway Proving Ground
ATTN: MT-S
Dugway, UT 84022

HQ, ESD/DRI/S-22
Hanscom AFB
MA 01731

Head, Atmospheric Rsch Section
National Science Foundation
1800 G. Street, NW
Washington, DC 20550

Office, Asst Sec Army (R&D)
ATTN: Dep for Science & Tech
HQ, Department of the Army
Washington, DC 20310

Commander
US Army Satellite Comm Agc
ATTN: DRCPM-SC-3
Fort Monmouth, NJ 07703

Sylvania Elec Sys Western Div
ATTN: Technical Reports Library
PO Box 205
Mountain View, CA 94040

William Peterson
Research Association
Utah State University, UNC 48
Logan, UT 84322

Defense Communications Agency
Technical Library Center
Code 205
Washington, DC 20305

Dr. A. D. Belmont
Research Division
PO Box 1249
Control Data Corp
Minneapolis, MN 55440

Commander
US Army Electronics Command
ATTN: DRSEL-WL-D1
Fort Monmouth, NJ 07703

Commander
ATTN: DRSEL-VL-D
Fort Monmouth, NJ 07703

Meteorologist in Charge
Kwajalein Missile Range
PO Box 67
APO
San Francisco, CA 96555

The Library of Congress
ATTN: Exchange & Gift Div
Washington, DC 20540
2

US Army Liaison Office
MIT-Lincoln Lab, Library A-082
PO Box 73
Lexington, MA 02173

Dir National Security Agency
ATTN: TDL (C513)
Fort George G. Meade, MD 20755

Director, Systems R&D Service
Federal Aviation Administration
ATTN: ARD-54
2100 Second Street, SW
Washington, DC 20590

Commander
US Army Missile Command
ATTN: DRSMI-RRA, Bldg 7770
Redstone Arsenal, AL 35809

Dir of Dev & Engr
Defense Systems Div
ATTN: SAREA-DE-DDR
H. Tannenbaum
Edgewood Arsenal, APG, MD 21010

Naval Surface Weapons Center
Technical Library & Information
Services Division
White Oak, Silver Spring, MD
20910

Dr. Frank D. Eaton
PO Box 3038
Universtiy Station
Laramie, Wyoming 82071

Rome Air Development Center
ATTN: Documents Library
TILD (Bette Smith)
Griffiss Air Force Base, NY 13441

National Weather Service
National Meteorological Center
World Weather Bldg - 5200 Auth Rd
ATTN: Mr. Quiroz
Washington, DC 20233

USAFETAC/CB (Stop 825)
Scott AFB
IL 62225

Director
Defense Nuclear Agency
ATTN: Tech Library
Washington, DC 20305

Director
Development Center MCDEC
ATTN: Firepower Division
Quantico, VA 22134

Environmental Protection Agency
Meteorology Laboratory
Research Triangle Park, NC
27711

Commander
US Army Electronics Command
ATTN: DRSEL-GG-TD
Fort Monmouth, NJ 07703

Commander
US Army Ballistic Rsch Labs
ATTN: DRXBR-IB
APG, MD 21005

Dir, US Naval Research Lab
Code 5530
Washington, DC 20375

Mil Assistant for
Environmental Sciences
DAD (E & LS), 3D129
The Pentagon
Washington, DC 20301

The Environmental Rsch
Institute of MI
ATTN: IRIA Library
PO Box 618
Ann Arbor, MI 48107

Armament Dev & Test Center
ADTC (DLOSL)
Eglin AFB, Florida 32542

Range Commanders Council
ATTN: Mr. Hixon
PMTC Code 3252
Pacific Missile Test Center
Point Mugu, CA 93042

Commander
Eustis Directorate
US Army Air Mobility R&D Lab
ATTN: Technical Library
Fort Eustis, VA 23604

Commander
Frankford Arsenal
ATTN: SARFA-FCD-O, Bldg 201-2
Bridge & Tarcony Sts
Philadelphia, PA 19137

Director, Naval Oceanography and
Meteorology
National Space Technology Laboratories
Bay St Louis, MS 39529

Commander
US Army Electronics Command
ATTN: DRSEL-CT-S
Fort Monmouth, NJ 07703

Commander
USA Cold Regions Test Center
ATTN: STECR-OP-PM
APO Seattle 98733

Redstone Scientific Information Center
ATTN: DRDMI-TBD
US Army Missile Res & Dev Command
Redstone Arsenal, AL 35809

Commander
AFWL/WE
Kirtland AFB, NM 87117

Naval Surface Weapons Center
Code DT-22 (Ms. Greeley)
Dahlgren, VA 22448

Commander
Naval Ocean Systems Center
ATTN: Research Library
San Diego, CA 92152

Commander
US Army INSCOM
ATTN: IARDA-OS
Arlington Hall Station
Arlington, VA 22212

Commandant
US Army Field Artillery School
ATTN: ATSF-CF-R
Fort Sill, OK 73503

Commander and Director
US Army Engineer Topographic Labs
ETL-GS-AC
Fort Belvoir, VA 22060

Technical Processes Br-D823
NOAA, Lib & Info Serv Div
6009 Executive Blvd
Rockville, MD 20852

Commander
US Army Missile Research
and Development Command
ATTN: DRDMI-CGA, B. W. Fowler
Redstone Arsenal, AL 35809

Commanding Officer
US Army Armament Rsch & Dev Com
ATTN: DRDAR-TSS #59
Dover, NJ 07801

Air Force Cambridge Rsch Labs
ATTN: LCB (A. S. Carten, Jr.)
Hanscom AFB
Bedford, MA 01731

National Center for Atmos Res
NCAR Library
PO Box 3000
Boulder, CO 80307

Air Force Geophysics Laboratory
ATTN: LYD
Hanscom AFB
Bedford, MA 01731

Chief, Atmospheric Sciences Division
Code ES-81
NASA
Marshall Space Flight Center, AL 35812

Department of the Air Force
OL-C, 5WW
Fort Monroe, VA 23651

Commander
US Army Missile Rsch & Dev Com
ATTN: DRDMI-TR
Redstone Arsenal, AL 35809

Meteorology Laboratory
AFGL/LY
Hanscom AFB, MA 01731

Director CFD
US Army Field Artillery School
ATTN: Met Division
Fort Sill, OK 73503

Naval Weapons Center (Code 3173)
ATTN: Dr. A. Shlanta
China Lake, CA 93555

Director
Atmospheric Physics & Chem Lab
Code R31, NOAA
Department of Commerce
Boulder, CO 80302

Department of the Air Force
5 WW/DN
Langley AFB, VA 23665

Commander
US Army Intelligence Center and School
ATTN: ATSI-CD-MD
Fort Huachuca, AZ 85613

Dr. John L. Walsh
Code 4109
Navy Research Lab
Washington, DC 20375

Director
US Army Armament Rsch & Dev Com
Chemical Systems Laboratory
ATTN: DRDAR-CLJ-I
Aberdeen Proving Ground, MD 21010

R. B. Girardo
Bureau of Reclamation
E&R Center, Code 1220
Denver Federal Center, Bldg 67
Denver, CO 80225

Commander
US Army Missile Command
ATTN: DRDMI-TEM
Redstone Arsenal, AL 35809

Commander
US Army Tropic Test Center
ATTN: STETC-MO (Tech Library)
APO New York 09827

Commanding Officer
Naval Research Laboratory
Code 2627
Washington, DC 20375

Defense Documentation Center
ATTN: DDC-TCA
Cameron Station (Bldg 5)
Alexandria, Virginia 22314
12

Commander
US Army Test and Evaluation Command
ATTN: Technical Library
White Sands Missile Range, NM 88002

US Army Nuclear Agency
ATTN: MONA-WE
Fort Belvoir, VA 22060

Commander
US Army Proving Ground
ATTN: Technical Library
Bldg 2100
Yuma, AZ 85364

Office, Asst Sec Army (R&D)
ATTN: Dep for Science & Tech
HQ, Department of the Army
Washington, DC 20310

ATMOSPHERIC SCIENCES RESEARCH PAPERS

1. Lindberg, J.D., "An Improvement to a Method for Measuring the Absorption Coefficient of Atmospheric Dust and other Strongly Absorbing Powders, " ECOM-5565, July 1975.
2. Avara, Elton, P., "Mesoscale Wind Shears Derived from Thermal Winds," ECOM-5566, July 1975.
3. Gomez, Richard B., and Joseph H. Pierluissi, "Incomplete Gamma Function Approximation for King's Strong-Line Transmittance Model," ECOM-5567, July 1975.
4. Blanco, A.J., and B.F. Engebos, "Ballistic Wind Weighting Functions for Tank Projectiles," ECOM-5568, August 1975.
5. Taylor, Fredrick J., Jack Smith, and Thomas H. Pries, "Crosswind Measurements through Pattern Recognition Techniques," ECOM-5569, July 1975.
6. Walters, D.L., "Crosswind Weighting Functions for Direct-Fire Projectiles," ECOM-5570, August 1975.
7. Duncan, Louis D., "An Improved Algorithm for the Iterated Minimal Information Solution for Remote Sounding of Temperature," ECOM-5571, August 1975.
8. Robbiani, Raymond L., "Tactical Field Demonstration of Mobile Weather Radar Set AN/TPS-41 at Fort Rucker, Alabama," ECOM-5572, August 1975.
9. Miers, B., G. Blackman, D. Langer, and N. Lorimier, "Analysis of SMS/GOES Film Data," *ECOM-5573, September 1975.*
10. Manquero, Carlos, Louis Duncan, and Rufus Bruce, "An Indication from Satellite Measurements of Atmospheric CO2 Variability," ECOM-5574, September 1975.
11. Petracca, Carmine, and James D. Lindberg, "Installation and Operation of an Atmospheric Particulate Collector," ECOM-5575, September 1975.
12. Avara, Elton P., and George Alexander, "Empirical Investigation of Three Iterative Methods for Inverting the Radiative Transfer Equation," ECOM-5576, October 1975.
13. Alexander, George D., "A Digital Data Acquisition Interface for the SMS Direct Readout Ground Station — Concept and Preliminary Design," ECOM-5577, October 1975.
14. Cantor, Israel, "Enhancement of Point Source Thermal Radiation Under Clouds in a Nonattenuating Medium," ECOM-5578, October 1975.
15. Norton, Colburn, and Glenn Hoidale, "The Diurnal Variation of Mixing Height by Month over White Sands Missile Range, N.M," ECOM-5579, November 1975.
16. Avara, Elton P., "On the Spectrum Analysis of Binary Data," ECOM-5580, November 1975.
17. Taylor, Fredrick J., Thomas H. Pries, and Chao-Huan Huang, "Optimal Wind Velocity Estimation," ECOM-5581, December 1975.
18. Avara, Elton P., "Some Effects of Autocorrelated and Cross-Correlated Noise on the Analysis of Variance, " ECOM-5582, December 1975.
19. Gillespie, Patti S., R.L. Armstrong, and Kenneth O. White, "The Spectral Characteristics and Atmospheric CO2 Absorption of the Ho^{+3}:YLF Laser at 2.05μm," ECOM-5583, December 1975.
20. Novlan, David J. "An Empirical Method of Forecasting Thunderstorms for the White Sands Missile Range," ECOM-5584, February 1976.
21. Avara, Elton P., "Randomization Effects in Hypothesis Testing with Autocorrelated Noise," ECOM-5585, February 1976.
22. Watkins, Wendell R., "Improvements in Long Path Absorption Cell Measurement," ECOM-5586, March 1976.
23. Thomas, Joe, George D. Alexander, and Marvin Dubbin, "SATTEL — An Army Dedicated Meteorological Telemetry System," ECOM-5587. March 1976.
24. Kennedy, Bruce W., and Delbert Bynum, "Army User Test Program for the RDT&E-XM-75 Meteorological Rocket," ECOM-5588, April 1976.

25. Barnett, Kenneth M., "A Description of the Artillery Meteorological Comparisons at White Sands Missle Range, October 1974 - December 1974 ('PASS' - Prototype Artillery [Meteorological] Subsystem)," ECOM-5589, April 1976.
26. Miller, Walter B., "Preliminary Analysis of Fall-of-Shot From Project 'PASS'," ECOM-5590, April 1976.
27. Avara, Elton P., "Error Analysis of Minimum Information and Smith's Direct Methods for Inverting the Radiative Transfer Equation," ECOM-5591, April 1976.
28. Yee, Young P., James D. Horn, and George Alexander, "Synoptic Thermal Wind Calculations from Radiosonde Observations Over the Southwestern United States," ECOM-5592, May 1976.
29. Duncan, Louis D., and Mary Ann Seagraves, "Applications of Empirical Corrections to NOAA-4 VTPR Observations," ECOM-5593, May 1976.
30. Miers, Bruce T., and Steve Weaver, "Applications of Meterological Satellite Data to Weather Sensitive Army Operations,"ECOM-5594, May 1976.
31. Sharenow, Moses, "Redesign and Improvement of Balloon ML-566," ECOM-5595, June, 1976.
32. Hansen, Frank V., "The Depth of the Surface Boundary Layer," ECOM-5596, June 1976.
33. Pinnick, R.G., and E.B. Stenmark, "Response Calculations for a Commercial Light-Scattering Aerosol Counter," ECOM-5597, July 1976.
34. Mason, J., and G.B. Hoidale, "Visibility as an Estimator of Infrared Transmittance," ECOM-5598, July 1976.
35. Bruce, Rufus E., Louis D. Duncan, and Joseph H. Pierluissi, "Experimental Study of the Relationship Between Radiosonde Temperatures and Radiometric-Area Temperatures," ECOM-5599, August 1976.
36. Duncan, Louis D., "Stratospheric Wind Shear Computed from Satellite Thermal Sounder Measurements," ECOM-5800, September 1976.
37. Taylor, F., P. Mohan, P. Joseph and T. Pries, "An All Digital Automated Wind Measurement System," ECOM-5801, September 1976.
38. Bruce, Charles, "Development of Spectrophones for CW and Pulsed Radiation Sources," ECOM-5802, September 1976.
39. Duncan, Louis D., and Mary Ann Seagraves,"Another Method for Estimating Clear Column Radiances," ECOM-5803, October 1976.
40. Blanco, Abel J., and Larry E. Taylor, "Artillery Meteorological Analysis of Project Pass," ECOM-5804, October 1976.
41. Miller, Walter, and Bernard Engebos," A Mathematical Structure for Refinement of Sound Ranging Estimates," ECOM-5805, November, 1976.
42. Gillespie, James B., and James D. Lindberg, "A Method to Obtain Diffuse Reflectance Measurements from 1.0 to 3.0 μm Using a Cary 17I Spectrophotometer," ECOM-5806, November 1976.
43. Rubio, Roberto, and Robert O. Olsen,"A Study of the Effects of Temperature Variations on Radio Wave Absorption,"ECOM-5807, November 1976.
44. Ballard, Harold N., "Temperature Measurements in the Stratosphere from Balloon-Borne Instrument Platforms, 1968-1975," ECOM-5808, December 1976.
45. Monahan, H.H., "An Approach to the Short-Range Prediction of Early Morning Radiation Fog," ECOM-5809, January 1977.
46. Engebos, Bernard Francis, "Introduction to Multiple State Multiple Action Decision Theory and Its Relation to Mixing Structures," ECOM-5810, January 1977.
47. Low, Richard D.H.,"Effects of Cloud Particles on Remote Sensing from Space in the 10-Micrometer Infrared Region," ECOM-5811, January 1977.
48. Bonner, Robert S., and R. Newton, "Application of the AN/GVS-5 Laser Rangefinder to Cloud Base Height Measurements," ECOM-5812, February 1977.
49. Rubio, Roberto, "Lidar Detection of Subvisible Reentry Vehicle Erosive Atmospheric Material," ECOM-5813, March 1977.
50. Low, Richard D.H., and J.D. Horn, "Mesoscale Determination of Cloud-Top Height: Problems and Solutions," ECOM-5814, March 1977.

51. Duncan, Louis D., and Mary Ann Seagraves,"Evaluation of the NOAA-4 VTPR Thermal Winds for Nuclear Fallout Predictions," ECOM-5815, March 1977.
52. Randhawa, Jagir S., M. Izquierdo, Carlos McDonald and Zvi Salpeter, "Stratospheric Ozone Density as Measured by a Chemiluminescent Sensor During the Stratcom VI-A Flight," ECOM-5816, April 1977.
53. Rubio, Roberto, and Mike Izquierdo, "Measurements of Net Atmospheric Irradiance in the 0.7- to 2.8-Micrometer Infrared Region," ECOM-5817, May 1977.
54. Ballard, Harold N., Jose M. Serna, and Frank P. Hudson Consultant for Chemical Kinetics, "Calculation of Selected Atmospheric Composition Parameters for the Mid-Latitude, September Stratosphere," ECOM-5818, May 1977.
55. Mitchell, J.D., R.S. Sagar, and R.O. Olsen, "Positive Ions in the Middle Atmosphere During Sunrise Conditions," ECOM-5819, May 1977.
56. White, Kenneth O., Wendell R. Watkins, Stuart A. Schleusener, and Ronald L. Johnson, "Solid-State Laser Wavelength Identification Using a Reference Absorber," ECOM-5820, June 1977.
57. Watkins, Wendell R., and Richard G. Dixon, "Automation of Long-Path Absorption Cell Measurements," ECOM-5821, June 1977.
58. Taylor, S.E., J.M. Davis, and J.B. Mason, "Analysis of Observed Soil Skin Moisture Effects on Reflectance," ECOM-5822, June 1977.
59. Duncan, Louis D. and Mary Ann Seagraves, "Fallout Predictions Computed from Satellite Derived Winds," ECOM-5823. June 1977.
60. Snider, D.E., D.G. Murcray, F.H. Murcray, and W.J. Williams, "Investigation of High-Altitude Enhanced Infrared Backround Emissions" (U), SECRET, ECOM-5824, June 1977.
61. Dubbin, Marvin H. and Dennis Hall, "Synchronous Meteorlogical Satellite Direct Readout Ground System Digital Video Electronics," ECOM-5825, June 1977.
62. Miller, W., and B. Engebos, "A Preliminary Analysis of Two Sound Ranging Algorithms," ECOM-5826, July 1977.
63. Kennedy, Bruce W., and James K. Luers, "Ballistic Sphere Techniques for Measuring Atomspheric Parameters," ECOM-5827, July 1977.
64. Duncan, Louis D., "Zenith Angle Variation of Satellite Thermal Sounder Measurements," ECOM-5828, August 1977.
65. Hansen, Frank V., "The Critical Richardson Number," ECOM-5829, September 1977.
66. Ballard, Harold N., and Frank P. Hudson (Compilers), "Stratospheric Composition Balloon-Borne Experiment," ECOM-5830, October 1977.
67. Barr, William C., and Arnold C. Peterson, "Wind Measuring Accuracy Test of Meteorological Systems," ECOM-5831, November 1977.
68. Ethridge, G.A. and F.V. Hansen, "Atmospheric Diffusion: Similarity Theory and Empirical Derivations for Use in Boundary Layer Diffusion Problems," ECOM-5832, November 1977.
69. Low, Richard D.H., "The Internal Cloud Radiation Field and a Technique for Determining Cloud Blackness," ECOM-5833, December 1977.
70. Watkins, Wendell R., Kenneth O. White, Charles W. Bruce, Donald L. Walters, and James D. Lindberg, "Measurements Required for Prediction of High Energy Laser Transmission," ECOM-5834, December 1977.
71. Rubio, Robert, "Investigation of Abrupt Decreases in Atmospherically Backscattered Laser Energy," ECOM-5835, December 1977.
72. Monahan, H.H. and R.M. Cionco, "An Interpretative Review of Existing Capabilities for Measuring and Forecasting Selected Weather Variables (Emphasizing Remote Means)," ASL-TR-0001, January 1978.
73. Heaps, Melvin G., "The 1979 Solar Eclipse and Validation of D-Region Models," ASL-TR-0002. March 1978.

74. Jennings, S.G., and J.B. Gillespie, "M.I.E. Theory Sensitivity Studies - The Effects of Aerosol Complex Refractive Index and Size Distribution Variations on Extinction and Absorption Coefficients Part II: Analysis of the Computational Results," ASL-TR-0003, March 1978.

☆ U.S. GOVERNMENT PRINTING OFFICE: 1977 777-093/ 36